Influence of membrane resistance on swelling and removal of colloidal filter cake after filtration pressure release

Maksym Loginov, Floriane Doudies, Nicolas Hengl, Frédéric Pignon, Geneviève Gésan-Guiziou

Influence of membrane resistance on swelling and removal of colloidal filter cake after filtration pressure release

Maksym Loginov[1,*], Floriane Doudiès[1], Nicolas Hengl[2], Frédéric Pignon[2], Geneviève Gésan-Guiziou[1]

[1]STLO, UMR 1253, INRA, Agrocampus Ouest, 35000 Rennes, France

[2]LRP, CNRS, Grenoble INP, Univeristé Grenoble Alpes, 38000 Grenoble, France

*Corresponding author (maksym.loginov@inra.fr; tel. +33 07 02 23 48 70 33)

Highlights

Impact of filtration membrane resistance on colloidal filter cake swelling is modeled
Possibility of filtrate uptake across the membrane during the swelling is considered
The lower is the membrane resistance the faster is the filter cake swelling
Concentration profile in the cake becomes bell-like when membrane resistance is low
Appearance of bell-like solid concentration profile can facilitate the cake removal

Abstract

The influence of filtration membrane resistance on colloidal filter cake swelling after the filtration pressure release is discussed in frame of filtration-consolidation theory. It is argued that in the case of reversibly compressible filter cake, the solid pressure relaxation can result in filtrate inflow across the membrane with the following absorption by the filter cake part adjacent to the membrane surface. According to the model results, the filtrate inflow and the filter cake swelling rates increase with decreasing of the membrane hydraulic resistance. At low membrane resistance, the swelling can result in the non-monotonous bell-like solid concentration distribution in the filter cake (solid concentration on the cake-membrane surface is lower than the maximal solid concentration). In contrast, the filter cake swelling in the absence of filter inflow across the membrane (or the deposit swelling on the impermeable surface) results in the monotonous decrease of the solid concentration. The non-monotonous solid concentration

distribution can facilitate the membrane rinsing and cleaning and lead to the filter cake removal before its complete swelling.

Keywords: filtration-consolidation theory, gel swelling, membrane rinsing, membrane fouling reversibility, membrane hydraulic resistance.

Nomenclature

C_e	modified average consolidation coefficient ($m^2 \cdot s^{-1}$)
c	local solid concentration ($kg \cdot m^{-3}$)
c_0	solid concentration in bulk suspension ($kg \cdot m^{-3}$)
c_{mi}	initial solid concentration on cake-membrane interface (at the end of filtration) ($kg \cdot m^{-3}$)
e	void ratio (dimensionless)
h	gap thickness, thickness of a layer on the membrane surface which can flow relatively the membrane and the rigid gel under the applied external shear stress (m)
K	parameter of Herschel-Bulkley equation ($Pa \cdot s^N$)
l	length (m)
N	parameter of Herschel-Bulkley equation (dimensionless)
ΔP	applied pressure (Pa)
p_l	liquid pressure (Pa)
p_m	solid pressure at the membrane surface (Pa)
p_{mi}	initial solid pressure at the membrane surface (at the end of filtration) (Pa)
p_s	compressive solid pressure (Pa)
p_{si}	initial solid pressure (at the end of filtration) (Pa)
r_{ci}	initial filter cake resistance (cake resistance at the end of filtration) (m^{-1})
r_{in}	outside-in membrane hydraulic resistance (m^{-1})
r_m	inside-out membrane hydraulic resistance (m^{-1})
r_r	hydraulic resistance of residual gel (m^{-1})
S	cross-sectional area of filtration membrane (m^2)
t	time (s)
U	completeness of filter cake swelling (dimensionless)
u	apparent liquid velocity relative to solids ($m \cdot s^{-1}$)

58 V_f filtrate volume (m^3)
59 $V_{f\infty}$ final filtrate volume (m^3)
60 v tangential velocity of rigid gel relative to membrane ($m \cdot s^{-1}$)
61 x distance to membrane surface in Cartesian coordinates (m)

62 **Greek letters**
63 α specific filtration resistance ($m \cdot kg^{-1}$)
64 α_e average specific filtration resistance at the membrane surface ($m \cdot kg^{-1}$)
65 α_m specific filtration resistance of a layer on a cake-membrane interface ($m \cdot kg^{-1}$)
66 $\dot{\gamma}$ shear rate (s^{-1})
67 θ required swelling duration, duration of swelling required in order to attain $\varphi_m = \varphi_{sg}$ (s)
68 κ local permeability (m^2)
69 λ variable, root of Eq. (A5) (dimensionless)
70 μ filtrate viscosity (Pa·s)
71 ξ variable (dimensionless)
72 ρ_s specific weight of solids ($kg \cdot m^{-3}$)
73 τ_0 local yield stress (Pa)
74 τ_{ext} external applied shear stress (wall shear stress) (Pa)
75 φ solid volume fraction (dimensionless)
76 φ_m solid volume fraction on cake-membrane interface (dimensionless)
77 φ_{max} maximal instant solid volume fraction in the system (dimensionless)
78 φ_{sg} solid volume fraction of sol-gel transition (dimensionless)
79 ω distance to membrane surface in material coordinates (m)
80 ω_0 position of cake-bulk interface in material coordinates (m)
81 ω_r thickness of swelled gel in material coordinates (m)
82

1. Introduction

In the literature, it is commonly accepted to distinguish two components of the external membrane fouling (fouling resistance): reversible fouling (which is removed from the surface by shear after the filtration pressure release/decrease or after the increasing of the shear rate) and irreversible fouling (that corresponds to the difference between the total fouling resistance and the resistance of reversible fouling). The scientific background for this distinction is DLVO theory applied to the case of a filter cake [1-4]. Increasing of the local compressive pressure applied to cake particles (solid pressure) in the direction of membrane surface results in the decreasing of local inter-particle distance (increasing of local particle concentration). At the distance to membrane surface, where the local compressive force overcomes the interparticle repulsion force, cake particles undergo an aggregation (sol-gel transition). In contrast to outer part of the cake (sol, concentration polarization layer), the inner part of the cake (rigid gel, deposit) is not removed from the membrane surface by crossflow shear until the shear force overcomes the particle attraction force (Coulomb failure criterion applied to filter cake removal [5]). Therefore, appearance of irreversible external membrane fouling is associated with the gel (or deposit, dense structure) formation on membrane surface.

The extent of irreversible membrane fouling is commonly characterized with the help of cyclic variation of filtration conditions: applied wall shear stress and transmembrane pressure (or imposed filtrate flux) [5-11]. The hysteresis of fouling, which is observed in coordinates fouling-resistance vs. pressure (or vs. shear stress), is used in order to determine critical fouling conditions (filtration conditions that result in gel formation). It should be noticed that duration of filtration cycles (fouling formation followed by fouling removal) is typically short, and its influence on results of the experiment (extent of irreversible fouling, irreversibility of fouling in general) is out of the scope of the majority of studies.

However, a number of articles demonstrated that both the rate and the extent of fouling removal after a cross-flow and dead-end filtration increases with the increasing of duration of the pressure relaxation step [11-18]. In other words, sufficient pressure relaxation duration can result in the following removal of “irreversible” fouling (at least partial). For example, it was demonstrated that the casein micelles gel, which is considered to cause irreversible fouling during the dead-end filtration-stirring experiment [19], can swell and redisperse in course of time after the osmotic compression experiments [20] or in a different filtration experiment [21].

Articles concerning the modelling of the influence of pressure relaxation duration on the fouling extent and removal rate are rather rare in filtration literature [18]. However, significant progress is attained in the modelling of gel dissolution and the hydrodynamic cleaning (i.e., rinsing) of impermeable surface from foulants (deposits), where models consider the time-dependent gel swelling (solvent diffusion into a deposit) that precedes the particles/molecules redispersion by applied flow (e.g., [22-36]). In addition, behavior of filter cakes (and consolidated filter cakes) after the filtration pressure decrease (or release) was modeled in the frame of conventional filtration-consolidation theory and experimentally characterized in a series of papers by Iritani, Iwata, Katagiri, Murase, and Shirato [37-45] and Banks [46]. Particularly, it was experimentally demonstrated that colloidal filter cakes (and hydrogels) can swell and restore lower values of local particle concentration and permeability (at least partially) after the filtration pressure release [40, 42-45] and a new definition of filter cake reversibility, based on filtration resistance recovery, was introduced [44]. It was demonstrated that the response of filter cake properties (accessed from the experimentally measured filter cake resistance) on the variation of applied pressure is not immediate, and kinetics of cake relaxation is related with local cake properties (compressibility and permeability), initial cake thickness and values of compressive pressure applied during the filter cake formation and cake relaxation [37-45]. Unfortunately, previous articles did not take into consideration any possible influence of filtration membrane resistance on the filter cake relaxation and the following membrane rinsing.

The present article is devoted to the modeling of colloidal filter cake swelling after the filtration pressure release in the frame of filtration-consolidation theory. It is assumed that the filter cake compression is reversible, in particular, the local filter cake concentration can decrease below the concentration of sol-gel transition during the swelling. In this case, the sol-gel transition is defined as the transition from liquid-like to solid-like rheological behavior. The present article considers the influence of the membrane resistance to filtrate inflow into the cake on the cake swelling kinetics, and analyzes the influence of parameters (the filter cake thickness, compressibility and permeability, the membrane hydraulic resistance, the swelling duration, flow behavior of swelled material) on the following membrane rinsing by tangential shear. Several possible methods for the experimental verification of model results are proposed and the importance of swelling duration and membrane resistance for the fouling removal is discussed.

2. Description of a filter cake swelling on membrane surface

When a liquid flows across a porous body under a pressure difference ΔP (e.g., across a filter cake and a membrane during a constant pressure dead-end filtration of particulate suspension, Fig. 1a), the liquid pressure p_l in capillaries between particles and in membrane pores decreases in the flow direction.

Fig. 1a,b.

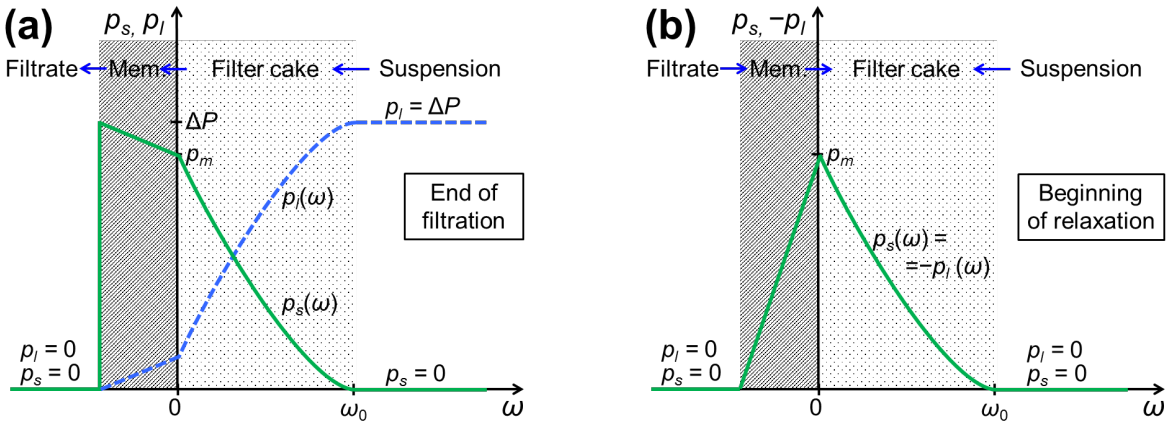

Fig. 1. Liquid p_l and solid p_s pressures (dashed and solid curves, respectively) in a system of a particulate filter cake on a membrane surface at the moments (a) before and (b) after the release of filtration pressure ΔP; arrows show the liquid flow direction. The initial solid pressure in the cake p_{si} varies from the membrane-cake ($\omega = 0$) to the cake-suspension interface ($\omega = \omega_0$), where is ω the material coordinate. For colloidal objects, distribution of the local osmotic pressure π in cake and suspension is equivalent to distribution of p_s in particulate filter cake, while the liquid pressure p_l is not determined.

The liquid pressure decreases because of the friction (viscous drag), which exists between the moving liquid and stationary particles (pores surface). The same force with an opposite sign is exerted on solids by the moving liquid. In the conventional filtration-consolidation theory, the net force applied to particles or porous body is divided by the cross-sectional area of the whole system and represented as an effective (fictive) solid compressive pressure p_s (e.g., [47]). In the case of the pressure filtration, the local force balance (i.e., force balance in a thin cross-sectional

layer of the filter cake or filtration membrane) is presented by Eq. (1):

$$\mathrm{d}p_s = -\mathrm{d}p_l \tag{1}$$

Eq. (1) is used in the majority of pressure filtration models [47-49]. Given that in suspension $p_l = \Delta P$ and $p_s = 0$ (there is no relative solid-liquid movement and friction), integration of Eq. (1) across the system of a filter cake and filtration membrane yields

$$\Delta P = p_l + p_s \tag{2}$$

Eqs. (1) implies that p_s increases with decreasing of p_l (in the flow direction, Fig. 1a). The solid compressive pressure increases because the compressive force is transmitted and accumulated in the flow direction across the porous body (from particle to particle, from filter cake to membrane, and along the membrane pores). At the given moment of filtration, the solid pressure within the cake increases from zero at the cake-suspension interface to a maximum at the cake-membrane interface (which is denoted herein as p_m). It further increases across the membrane (linearly with the depth, if the membrane is homogeneous and incompressible) and reaches $p_s = \Delta P$ at the external membrane surface. In filtrate, both $p_l = 0$ and $p_s = 0$ because the applied pressure is transmitted to a membrane support (Fig. 1a).

Eq. (1) allows substituting the liquid pressure gradient $\mathrm{d}p_l/\mathrm{d}x$ in the Darcy equation

$$u \propto \mathrm{d}p_l/\mathrm{d}x \tag{3}$$

with the solid pressure gradient $\mathrm{d}p_s/\mathrm{d}x$ and applying the Darcy equation for description of liquid flow in compressible filter cakes (i.e., filter cakes with p_s-dependent permeability and particle concentration):

$$u = -\frac{1}{\mu\alpha(p_s)\rho_s}\frac{\mathrm{d}p_s}{\mathrm{d}\omega} \tag{4}$$

where u is the apparent liquid velocity relative to solids, μ is liquid viscosity, α is local specific resistance, ρ_s is density of the solids, ω is material coordinate. Therefore, Eq. (4) is widely used for description of formation and consolidation of particulate filter cakes [47-49].

Usually, membrane filtration of colloidal objects that have a considerable osmotic pressure π is not discussed in terms of local values of p_l and p_s, which characterize porous bodies and particulate filter cakes; in this case Eq. (4) can not be applied immediately. However, Elimelech and Bhattacharjee [50] demonstrated that the drag force, which is applied by moving liquid to a layer of colloidal particles or solute molecules retained by the membrane during filtration is equal to a thermodynamic force, which is exerted by solvent molecules on these particles (solute

molecules). The thermodynamic force is related with the solvent chemical potential (and not with the solvent pressure alone as the drag force applied to the liquid in conventional filtration-consolidation theory for particulate and porous systems), and it is directly proportional to a local osmotic pressure gradient $d\pi/dx$ [50]. Since the drag force is directly proportional to the apparent liquid velocity u (according to Stokes equation), it follows that

$$u \propto -d\pi/dx \tag{5}$$

during the liquid flow across the layer of colloidal particles (solute molecules) [50]. Eq. (5) can be transformed into Eq. (4), where p_s stands for π and local properties of colloidal particle layer are characterized in terms of conventional filtration-consolidation theory (specific cake resistance and solid volume fraction) instead of collective diffusion coefficient and number particle concentration, which are usually employed for description of colloids with considerable osmotic pressure. That is why Eq. (4) was applied for description of membrane filtration and consolidation of colloids with considerable osmotic pressure and without a defined capillary structure: protein solutions [51] and hydrogel particles (polymer networks) [52, 53]. Distribution of π during filtration of colloidal objects is equivalent to distribution of p_s (which is presented in Fig. 1a), while p_l is usually not determined for colloidal filter cakes.

For majority of materials the increasing of solid pressure causes the filter cake compression, i.e., plastic and elastic structure deformation and increasing of solids concentration (because of the decreasing of inter-particle distance together with deformation and squeezing of aggregates and porous particles). For many materials (especially, for colloids with considerable osmotic pressure, e.g., repulsing nanoparticles, polymer molecules, soft particles having elastic polymer networks), the structure deformation under compression can be reversible, at least partially. After release of the applied pressure, which maintained a solid pressure in the reversibly compressible filter cake, the remaining solid pressure tends to dissipate via the structure expansion, as a compressed spring after the load release. Consequently, the liquid flows inside the filter cake, the filter cake swells (expands) (Fig. 1b). In the case of reversibly compressible particulate filter cake, this liquid inflow can be seen as a result of the momentary liquid pressure reduction in the filter cake: after the release of ΔP, p_l in the filter cake becomes negative (relative to the atmospheric pressure) in accordance to Eq. (2). This decreasing of p_l can be seen as result of a tension created in liquid-filled pores and capillaries by expanding elastic solid structure of compressed particulate filter cake. In the case of reversibly compressible colloidal filter cakes

with considerable osmotic pressure, the liquid inflow after the pressure release can be seen as osmotic effect. The liquid is absorbed by colloidal filter cake because its excessive osmotic pressure (relative to the osmotic pressure of filtrate and bulk suspensions, which are assumed to be negligible herein) is not compensated by the applied pressure after the pressure release. In both cases, the liquid flows inside the cake, in the direction of higher solid compressive (or osmotic) pressure areas after the release of applied pressure (Fig. 1b).

Basic equations of filtration-consolidation theory (which are normally used to describe cake formation and compression [47, 54, 55]) hold to describe the filter cake swelling as well:

a) the continuity equation for the liquid flow in an infinitesimal layer of a filter cake

$$\left(\frac{\partial e}{\partial t}\right)_{\omega} = -\left(\frac{\partial u}{\partial \omega}\right)_{t} \tag{6}$$

(where t is time, ω is material coordinate, e is local void ratio, which is equal to porosity divided by solids volume fraction (see Eq. (B3) in Appendix B), u is the apparent liquid velocity relative to solids);

b) the Darcy equation (4);

c) and the force balance Eq. (1).

Their combination yields the basic consolidation equation [56]

$$\frac{\partial p_s}{\partial t} = -\frac{\partial p_s}{\partial e} \cdot \frac{\partial}{\partial \omega}\left(\frac{1}{\mu \rho_s \alpha}\frac{\partial p_s}{\partial \omega}\right) \tag{7}$$

which can describe the filter cake swelling, if appropriate initial and boundary conditions are used. In the case of colloidal filter cakes with considerable osmotic pressure, p_s in Eq. (7) and in the following discussion denotes π.

It should be underlined that derivation of Eq. (7) from Eq. (6) is based on the assumption that the local void fraction explicitly depends on the solid pressure only (and does not depend on time). Therefore, it is assumed that the filter cake behaves a Terzaghi element [52]; creep is not considered during the swelling in this model.

Fig. 1b presents the filter cake on the membrane surface at the moment of filtration pressure release. At end of filtration there is a certain solid pressure distribution within the filter cake – the initial solid pressure distribution in the swelling cake $p_{si}(\omega)$

$$p_s = p_{si}(\omega) \qquad \text{at } t = 0 \tag{8}$$

At the cake-suspension surface the solid pressure is naught (if suspension is diluted and the sample weight is negligible)

$$p_s = 0 \qquad \text{at } \omega = \omega_0 \tag{9}$$

At the moment after filtration pressure release the solid pressure at the cake-membrane surface p_m is maximal (as it was during the filter cake formation), while it is absent at the filtrate side of the membrane (Fig. 1b). It is reasonable to assume that during the swelling, the liquid (filtrate) can flow across the membrane into the filter cake under the solid pressure gradient, which is equal to p_m (this is also a usual presentation of osmotic flow across a semipermeable membrane). If it is assumed that membrane is a thin semipermeable incompressible continuum, this flow can be described using the Darcy equation as

$$u = \frac{p_m}{\mu r_{in}} \qquad \text{at } \omega = 0 \tag{10}$$

as soon as $p_s = 0$ in the filtrate. In Eq. (10), r_{in} is the outside-in membrane hydraulic resistance (resistance to the liquid flow across the membrane from the filtrate side into the cell). The value of r_{in} can differ from the value of the usually discussed inside-out membrane resistance r_m (e.g., [57]). The liquid flow also penetrates an infinitesimal filter cake layer adjacent to the membrane surface that can be described as

$$u = \frac{1}{\mu \alpha_m \rho_s} \frac{\mathrm{d}p_s}{\mathrm{d}\omega} \qquad \text{at } \omega = 0 \tag{11}$$

where α_m is specific resistance of this layer. Combination of Eqs. (10) and (11) yields the second boundary condition required for solution of Eq. (7):

$$\frac{\mathrm{d}p_s}{\mathrm{d}\omega} = \frac{\alpha_m \rho_s}{r_{in}} p_m \qquad \text{at } \omega = 0 \tag{12}$$

In Eq. (12) p_m and α_m change with time (decrease) during the swelling.

Eq. (12) differs the present paper from important works on the filter cake behavior after the filtration pressure release [37-39, 41, 42, 45, 46, 52], because previous models did not consider the membrane as a hindrance for filtrate inflow into the cake during the swelling (though the value of membrane resistance is usually included in the modeling of cake formation and cake expression [44, 51, 58-61]).

3. On the possibility of filtrate inflow and absorption across the membrane

In the previous section it was assumed that the liquid can flow inside the filter cake after the filtration pressure release due to the existence of solid pressure (or osmotic pressure) gradient across the semipermeable membrane. As it follows from Eqs. (1) and (2), this implies that the

liquid pressure in the membrane pores is negative $p_l < 0$ (relative to the atmospheric pressure in filtrate). In the case of particulate filter cakes, the liquid pressure is pores of relaxing cake is negative too (while the liquid pressure in osmotic systems is not determined). Surprisingly, the negative values of liquid pressure in relaxing filter cake or filtration membrane were not pointed out in previous studies on filter cakes expansion during the relaxation [37]. However, this phenomenon is recognized in discussions on osmotic flow across the semipermeable membrane [62, 63, 64, 65] and clay swelling in soil mechanics [66].

It is necessary to discuss the conditions, which enable the water flow across the membrane (and inside the particular filter cake) under the negative liquid pressure. Though purified and degassed water can exist for a certain time even at pressure below 0 Pa (i.e., under the tension above $1.01 \cdot 10^5$ Pa), it is expected that in a real case application of high tension to the liquid inside porous system will result in formation of cavities or dissolved gas bubbles [62, 65]. This would reduce the tension and interrupt or slow down the liquid transport across the membrane [62, 65, 67-69]. The probability of bubbles and cavities formation must be highly dependent on the actual membrane pore structure. We can speculate that it will less likely happen in very small pores (when the pore size is smaller than the critical size of bubble formation) and in membranes with large distant pores (when the actual liquid pressure gradient across the pore is lower that the liquid pressure gradient calculated from the nominal membrane resistance). In any case, the risk of bubbles formation and flow interruption increases with decreasing of the liquid tension (i.e., it increases with the increasing of the pressure applied during the filter cake formation ΔP). For this reason, all calculations in this article were performed for $\Delta P = 10^5$ Pa, which resulted in even lower maximal values of p_m and lower absolute values of p_l inside the membrane during the filter cake swelling (both depend on assumed filter cake thickness and membrane resistance).

4. Solution of basic consolidation equation for compressible filter cakes

Analytical solution of Eq. (7) for actual compressible filter cakes with pressure-dependent specific filtration resistance and void ratio is difficult to obtain. Therefore, these dependencies are usually substituted with a constant effective parameter (an average modified consolidation coefficient). Following this tradition, analytical solution of Eq. (7) with two constant effective parameters was obtained; the solution is presented and the reason of its restricted applicability is discussed in Appendix A.

Eq. (7) was also solved numerically for the actual case of compressible filter cakes, as it is discussed in Appendix B. The values of parameters (pressure dependencies of specific filtration resistance and solids volume fraction, local rheological properties, initial filter cake thickness, as well as applied pressure and membrane resistance) were typical for ultrafiltration of colloids that form highly compressible filter cakes with low permeability. Experimentally obtained constitutive equations for permeability, compressibility and shear stress of aqueous dispersions of casein micelles were used for this purpose; they are discussed in Appendix C.

Both solutions were obtained for a constant value of ω_0: it was assumed that the weight of solids in a filter cake holds during the swelling. This is a weak assumption for a filter cake that swells on horizontal membrane in the absence of agitation; the assumption means that the swelled part of the cake remains at the cake-suspension interface.

5. Results and discussion

5.1. Particle concentration distribution

Fig. 2 presents two examples of solution of Eq. (7): filter cake swelling kinetics without (a) and with (b) filtrate absorption across the membrane.

Fig. 2a, b.

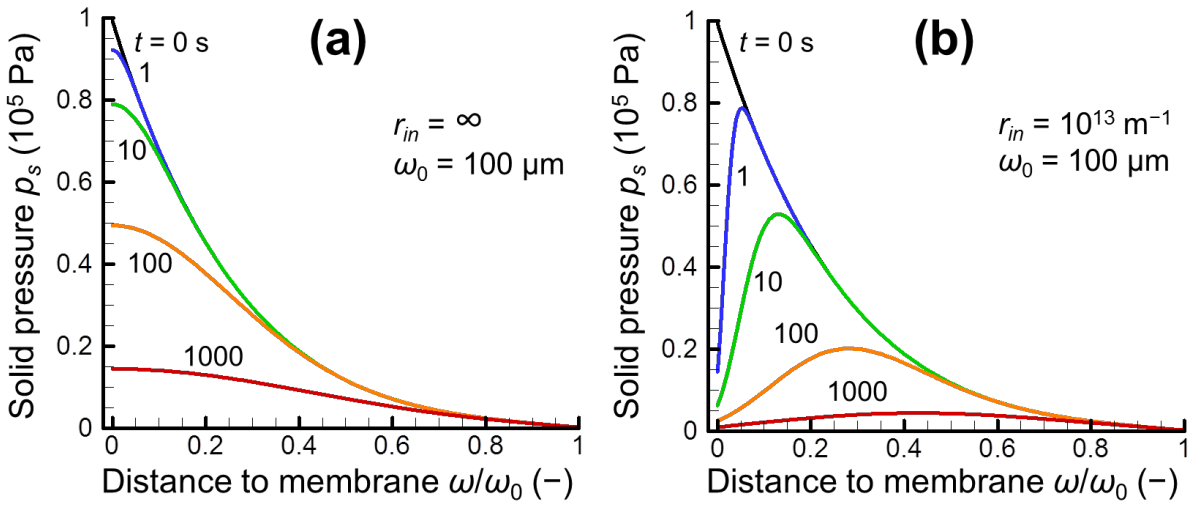

Fig. 2. Solid pressure distribution during the swelling of a thick filter cake (ω_0 = 100 μm) formed at the membrane surface with $r_m = 10^{13}$ m^{-1}: (a) without filtrate inflow across the membrane (r_{in} =

∞); (b) with filtrate inflow across the membrane with r_{in} = 10^{13} m^{-1}. The time after the pressure release (in seconds) is shown near the curves.

In the case when filtrate inflow into the cake does not happen for any reason (as it would be, for example, for impermeable surface, r_{in} = ∞), the solid pressure decreases continuously from the cake-membrane surface to the cake-bulk interface (Fig. 2a). However, when the membrane surface is permeable for filtrate, the solid pressure distribution in the swelling cake is non-monotonic (Fig. 2b), with the lower p_s values near the cake-membrane interface, which is explained by faster solid pressure relaxation in this area because of filtrate inflow across the membrane. Other observed trends (gradual decreasing of the solid pressure with time, slowdown of the pressure relaxation rate) are common for two cases and typical for relaxation processes. It must be noticed that in best of the authors' knowledge similar bell-like $p_s(\omega,t)$ behavior was for the first time reported by Murase [37] in the paper devoted to the modeling of expansion of consolidated material after the load release and later discussed in [39]. However, as soon as the membrane resistance was not considered (which is equal to the case r_{in} = 0), the solid pressure at the drainage (internal cake-membrane) surface attained p_s = 0 and the bell-like $p_s(\omega)$ and $\varphi(\omega)$ profiles appeared immediately on the beginning of cake expansion.

Fig. 3 presents the evolution of local solid concentration in the filter cake caused by the solid pressure decrease during the swelling with consideration of membrane resistance.

Fig. 3a – c.

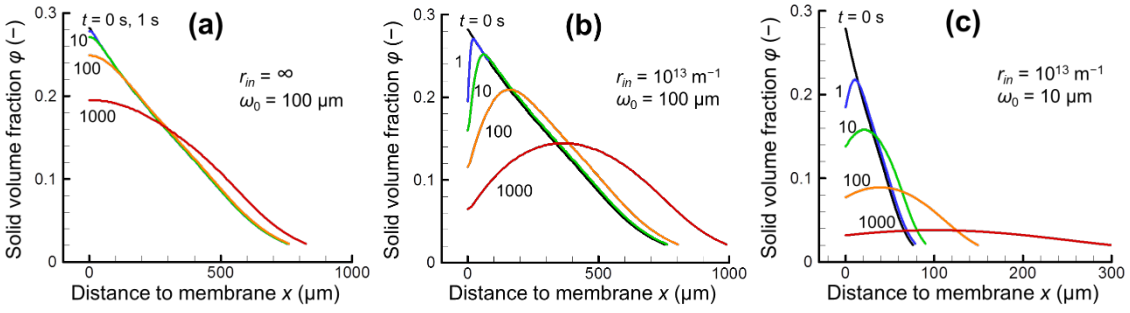

Fig. 3. Solid volume fraction distribution during the filter cake swelling: (a) thick filter cake without filtrate inflow across the membrane (r_{in} = ∞); (b) thick filter cake with filtrate inflow across the membrane with r_{in} = 10^{13} m^{-1}; (c) thin filter cake with filtrate inflow across the

membrane with $r_{in} = 10^{13}$ m^{-1}. The time after the pressure release (in seconds) is shown near the curves; in each case $r_m = 10^{13}$ m^{-1}.

In the absence of filtrate inflow across the membrane ($r_{in} = \infty$, Fig. 3a), the profiles $\varphi(x)$ have no peculiarities: monotonic decrease of solid pressure with x results in the monotonic decrease of particle concentration from the membrane surface to the cake-bulk interface. While in the case of filtrate inflow across the membrane (Figs. 3b,c), appearance of the low p_s area near the membrane results in the bell-like distribution of solid concentration, i.e., the maximal concentration is observed at a certain distance from the membrane; this distance increases with swelling duration. The maximum of the $\varphi(x)$ curve is more pronounced in the case of initially thick filter cake with $\omega_0 = 100$ μm as compared to thin cake with $\omega_0 = 10$ μm, which is explained by expectedly faster relaxation of thin cakes due to the faster liquid absorption across the cake-bulk interface. It can be noticed that in both cases ($r_{in} = \infty$ and $r_{in} \neq \infty$) the swelling of filter cakes results in rather small increase on the filter cake thickness at the beginning of the swelling ($t < 1000$ s), which can be difficult to detect by currently available methods for the filter cake surface visualization (e.g., optical coherence tomography [70], fluid dynamic gauging [71], electrochemical sensors [72], particle image velocimetry [73, 74], x-ray radiography [75], magnetic resonance imaging [76-78], ultrasonic [79], simple optical [80], etc. [81, 82]). However, the remarkable difference in local solid concentration distribution near the membrane surface in the case of thick filter cakes with and without filtrate inflow across the membrane could be observed, for example, by the method of *in situ* SAXS analysis of local solid concentration in filter cakes, described in [74, 83-85]. In the case of thin filter cakes, the available spatial resolution of SAXS (about 25 μm [86-88]) can be insufficient for observation of the bell-like shape of the $\varphi(x)$ [74]. Therefore, the general model verification requires an application of indirect methods of the filter cake analysis.

5.2. Particle concentration on membrane-cake interface

Fig. 4 presents the evolution of particle concentration on the internal membrane surface φ_m during the swelling of thick filter cakes at different values of membrane resistance r_{in}.

Fig. 4.

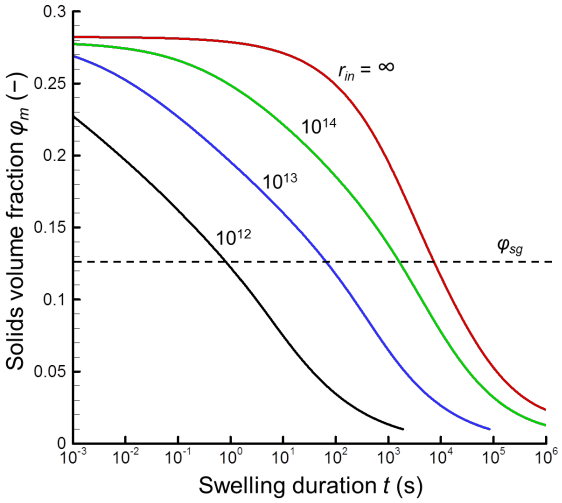

Fig. 4. Solid volume fraction at the cake-membrane interface versus the swelling duration for the thick filter cake (example for ω_0 = 100 μm) for different values of outside-in membrane resistance r_{in} (shown near the curves). The inside-out membrane resistance is $r_m = r_{in}$ (except of $r_m = 10^{13}$ m^{-1} for $r_{in} = \infty$). Dashed horizontal corresponds to the concentration of sol-gel transition φ_{sg} for the studied system.

For any nonzero value of membrane resistance (including $r_{in} = \infty$) the value of φ_m gradually decreases with time: the lower is r_{in}, the faster is the concentration decrease that is explained by faster filtrate inflow and its absorption by the filter cake part adjacent to the membrane surface. In the limiting case of $r_{in} = 0$, the solid volume fraction at the membrane surface decreases to the value $\varphi(p_s = 0)$ at the first instance of the swelling [37, 39]. However, in the current model it is assumed that the filter cake compression is reversible ($\varphi \to 0$ when $p_s \to 0$), and the value of φ_m can decrease below φ_{sg}, the concentration of sol-gel transition (i.e., transition from liquid-like to solid-like rheological behavior).

Fig. 5 presents the time θ, which is required in order to attain $\varphi_m = \varphi_{sg}$ at different conditions of swelling.

Fig. 5a – b.

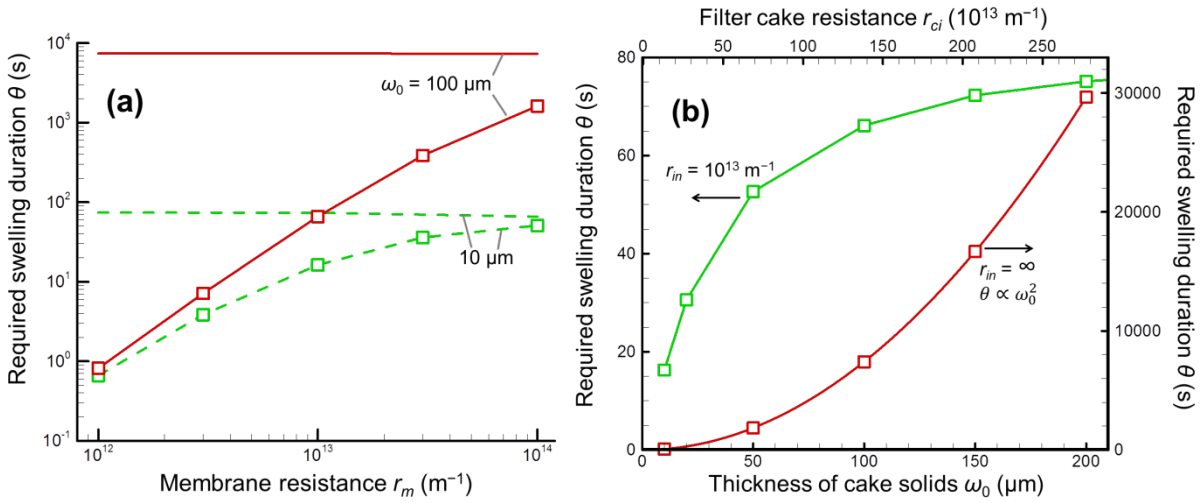

Fig. 5. Time required for filter cake swelling θ at different conditions: (a) θ versus the membrane hydraulic resistance r_m for thin (ω_0 = 10 µm, dashed curves) and thick (ω_0 = 100 µm, solid curves) filter cakes for the cases with ($r_{in} = r_m$, curves) and without ($r_{in} = \infty$, horizontals) filtrate inflow across the membrane; (b) θ versus the filter cake thickness ω_0 and initial filter cake resistance r_{ci} for the cases with (example for $r_{in} = 10^{13}$ m^{-1}) and without ($r_{in} = \infty$) filtrate inflow across the membrane with $r_m = 10^{13}$ m^{-1}.

For any filter cake thickness the value of θ increases with r_{in} and asymptotically approaches the value expected for the case of filter cake swelling in the absence of filtrate inflow across the membrane (cake swelling on impermeable surface with $r_{in} = \infty$, horizontals in Fig. 5a). The difference in swelling kinetics in the absence and presence of filtrate inflow is more remarkable for the thick filter cakes as compared to thin filter cakes. It is interesting to note that in the case when filtrate inflow is possible ($r_{in} \neq \infty$), the required swelling duration θ is far less sensitive to the filter cake thickness increase as compared to the case, when filtrate is not absorbed across the membrane ($r_{in} = \infty$). For example, when $r_{in} = 10^{13}$ m^{-1} the increasing of θ quickly slows down as ω_0 increases, while θ continuously increases as ω_0^2 in the case of impermeable membrane (Fig. 5b). This can be explained as follows: in first case the filtrate can be absorbed via two surfaces of the filter cake (Fig. 1), and its flow towards the high p_s area is impeded by membrane resistance r_{in} (which is assumed to be constant) and resistance of the filter cake r_{ci} (which is proportional to ω_0, Fig. 5b). Therefore, the increasing of r_{ci} in the case of a permeable membrane has only limited impact on the swelling kinetics at the membrane-cake interface. While in the

case of impermeable surface with $r_{in} = \infty$, the swelling follows the usual law for swelling and diffusion into a semi-infinite medium $t \propto l^2$ [53, 89].

5.3. Membrane rinsing after the filter cake swelling

It must be noticed that for any value of θ, when $\varphi_m = \varphi_{sg}$, the $\varphi(x)$ distribution in the swelling cake is distinct in case of the absence and presence of filtrate inflow across the membrane: in the case of $r_{in} = \infty$ the highest particle concentration exists at the membrane surface ($\varphi_{max} = \varphi_m = \varphi_{sg}$), while in the case with filtrate inflow φ_{max} is situated at the certain distance from the membrane surface and a gelled part of the filter cake with $\varphi_{max} > \varphi_{sg}$ remains in the system event when $t > \theta$. In principle, this difference can be used for the model verification via the following experiment. When a filter cake with $\varphi_m > \varphi_{sg}$ is present on the membrane, certain minimal value of tangential force is required in order to sweep it from the surface (e.g., [5]). It can be expected that both attraction between cake particles and adhesion of the cake to the membrane decrease with decreasing of local particle concentration [90-92] (for example, due to the swelling [12]). Below, it is assumed that the force, required for the sweeping of the filter cake layer with a local particle concentration φ, significantly decreases, when $\varphi \leq \varphi_{sg}$ (i.e., the gel is rigid and strongly attached to membrane surface, while the sol is liquid and can be easily removed). These are reasonable assumptions for a reversibly compressible filter cake, which is in the focus of the current paper. Fig. 6 schematically presents two filter cakes (after the swelling but before the rinsing): cake 1 with $\varphi_m > \varphi_{sg}$ and cake 2 with $\varphi_m < \varphi_{sg}$.

Fig. 6.

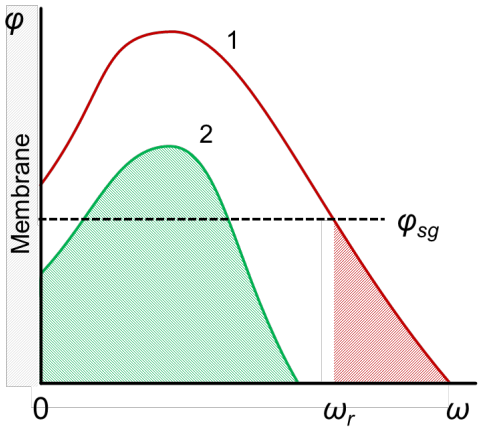

Fig. 6. To the experiment on membrane rinsing after the cake swelling: filter cakes with different particle concentration distribution (cake 1 with $\varphi_m > \varphi_{sg}$ and cake 2 with $\varphi_m < \varphi_{sg}$); dashed horizontal corresponds to the concentration of sol-gel transition, φ_{sg}, shaded parts can be removed from the surface (at left) by small tangential force, because $\varphi \le \varphi_{sg}$ at their left borders.

According to the previous reasoning, if small tangential force is applied, only shaded part of the cake 1 with $\varphi \le \varphi_{sg}$ is removed, the quantity of solids remaining on the membrane surface after the swelling-sweeping operation is defined by the solid pressure distribution profile attained during the sweeping and it is denoted as ω_r, $\omega_r > 0$ (Fig. 6). However, when the value $\varphi_m \le \varphi_{sg}$ is attained during the swelling (cake 2, Fig. 6), the cake is removed entirely because the adhesion of its part adjacent to membrane surface is small. If the hydraulic resistance of the residual part of the filter cake r_r is measured by liquid percolation at the same applied pressure ΔP as it was used for the cake formation, the value of r_r can be calculated as that of r_{ci} (using Eqs. (B8) – (B9) with the value of ω_0 replaced by ω_r).

Fig. 7a, b.

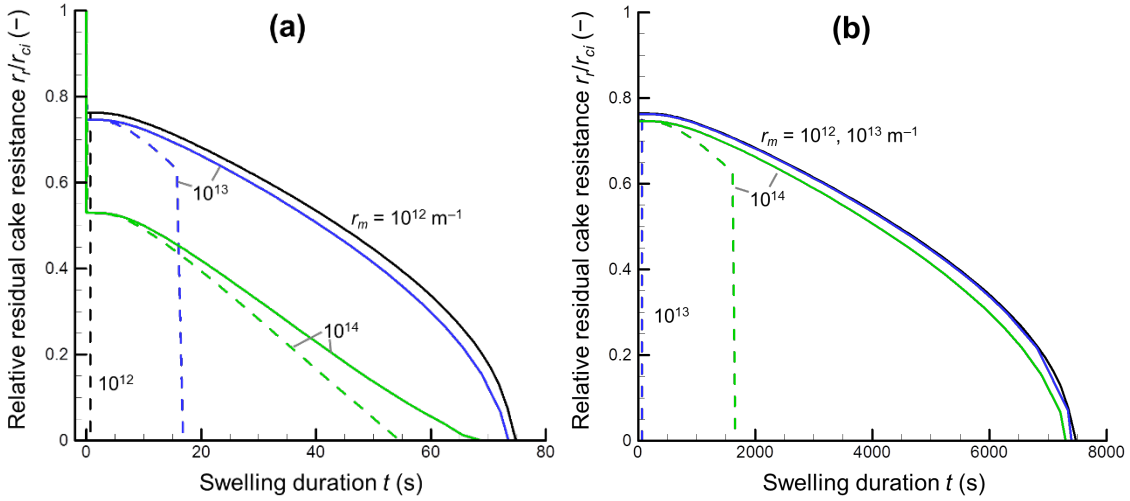

Fig. 7. Relative residual cake resistance r_r/r_{ci} when the sweeping force is applied after the swelling duration t in the absence (solid curves $r_{in} = \infty$) and presence (dashed curves, $r_{in} = r_m$) of filtrate inflow across the membrane: (a) thin filter cakes, ω_0 = 10 μm; (b) thick filter cakes, ω_0 = 100 μm. The values of r_m are shown near the curves.

Fig. 7a compares the values of r_r/r_{ci} attained after the swelling of initially thin (ω_0 = 10 μm) filter cakes different in the absence (solid curves) and presence (dashed curves) of filtrate inflow and absorption across the membrane. The observed immediate decrease of r_r/r_{ci} at t = 0 for all filter cakes is explained by the fact that the outer part of the cake has $\varphi < \varphi_{sg}$ and can be easily removed by sweeping without swelling. In the absence of filtrate inflow and absorption across the membrane ($r_{in} = \infty$), the difference in $r_r(t)$ behavior is explained by initially different filter cake structure, when the cakes are formed at different membrane resistances: the lower is r_m, the lower is the initial $\varphi(x)$ distribution (under constant ΔP and ω_0) and the faster is the cake swelling and removal (that corresponds to the small negative slope of horizontals in Fig. 5a). An important common feature for the cakes swelling at $r_{in} = \infty$ is that the decrease of $r_r(t)$ to 0 is gradual. In contrast, when the filtrate inflow and absorption across the membrane are possible, the $r_r(t)$ behavior is different: gradual decreasing is followed by an abrupt drop to 0, because at $t = \theta$ the gelled part of the swelling cake is not in a direct contact with the membrane. This difference is less obvious for thin filter cakes at high values of r_{in} (at low ratio of $r_{ci}/r_{in,}$ e.g. for $r_m = 10^{14}$ m^{-1} in Fig. 7a) because in this case the swelling behavior at large t approaches to that in the absence of filtrate inflow (Fig. 3c). However, this difference is distinct in the case of low r_{in} ($r_{in} = 10^{12}$ and 10^{13} m^{-1}). For thick cakes (ω_0 = 100 μm), which swell with filtrate inflow across the membrane, an abrupt drop of r_r is observed even in the case of high r_{in} (Fig. 7b).

Though an implementation of the experiment on the swelling followed by the sweeping described above can put in evidence the influence of the membrane resistance on the filter cake swelling kinetics, it is based on the assumption that the swelled gel (with $\varphi_m < \varphi_{sg}$) is instantaneously removed from the surface under the application of a small (infinitesimal) tangential shear force. However, in practice, removal of the swelled gel from the surface in a reasonably short time will require an application of certain minimal force. This can also provoke a tangential movement ("sliding") of the non-swelled gel that must be considered in predicting of the $r_r(t)$ behavior. It can be assumed that when an external tangential shear force τ_{ext} is applied to the gel after a certain swelling duration, the entire gel can move along the membrane surface in the direction of τ_{ext}, if a part of the swelled gel in vicinity of the membrane attained a concentration, which corresponds to the local yield stress $\tau_0 < \tau_{ext}$ (at x = 0..h, Fig. 8).

451 *Fig. 8.*

452

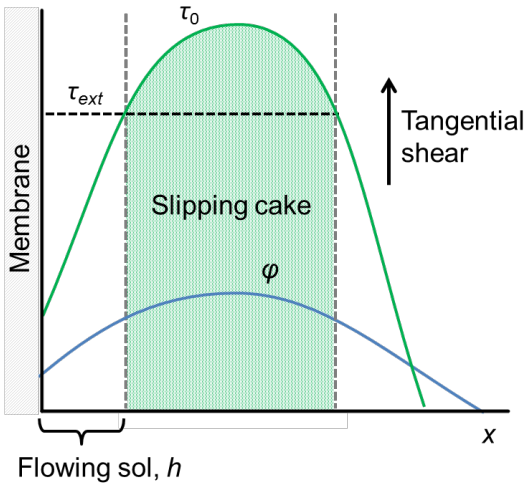

Fig. 8. Solid concentration distribution $\varphi(x)$ and corresponding yield stress distribution $\tau_0(x)$ in a swelled gel. In the vicinity of membrane the part of the gel with $\tau_0(x) < \tau_{ext}$ can flow under the external shear force, that cause the movement of the denser part of the gel with $\tau_0(x) > \tau_{ext}$.

453 If it is assumed that the part of the gel having local yield stress $\tau_0(x) > \tau_{ext}$ behaves as a rigid body
454 (shaded area in Fig. 8), its velocity can be estimated from the equation for the plate, which moves
455 relatively a parallel fixed surface (membrane) with the gap filled with non-Newtonian liquid
456 having rheological properties depending on a local solid concentration. If the local rheological
457 properties in flowing sol (Fig. 8) are described by Herschel-Bulkley model (Eq. (C3)), the
458 relative velocity v under the external shear stress τ_{ext} can be calculated as

$$v = \int_0^h \left(\frac{\tau_{ext} - \tau_0(x)}{K(x)} \right)^{\frac{1}{N(x)}} \mathrm{d}x \tag{13}$$

459 where h is the thickness of the gap between the membrane and the gel ($\tau_0 = \tau_{ext}$ at $x = h$, Fig. 8),
460 and the local values of parameters of Herschel-Bulkley equation $K(x)$, $N(x)$ and $\tau_0(x)$ are
461 determined by the local solid concentration $\varphi(x)$.

462 Fig. 9 presents values of the gap thickness h and the velocity v calculated for different
463 swelling durations t. The concentration dependencies of Herschel-Bulkley equation parameters,
464 determined by Jin et al. [83] for casein micelles dispersion and presented in the Appendix C,
465 were used for calculations. The data presented in Fig. 9 are calculated for $\tau_{ext} = 20$ Pa, which is a

reasonable estimate for the upper level of τ_{ext} available for conventional lab scale tangential and stirred dead-end filtration equipment. At the same time τ_{ext} = 20 Pa is significantly lower than the yield stress of the gelled part of the filter cake on the membrane surface before the swelling (Fig. C2)

Fig. 9a, b.

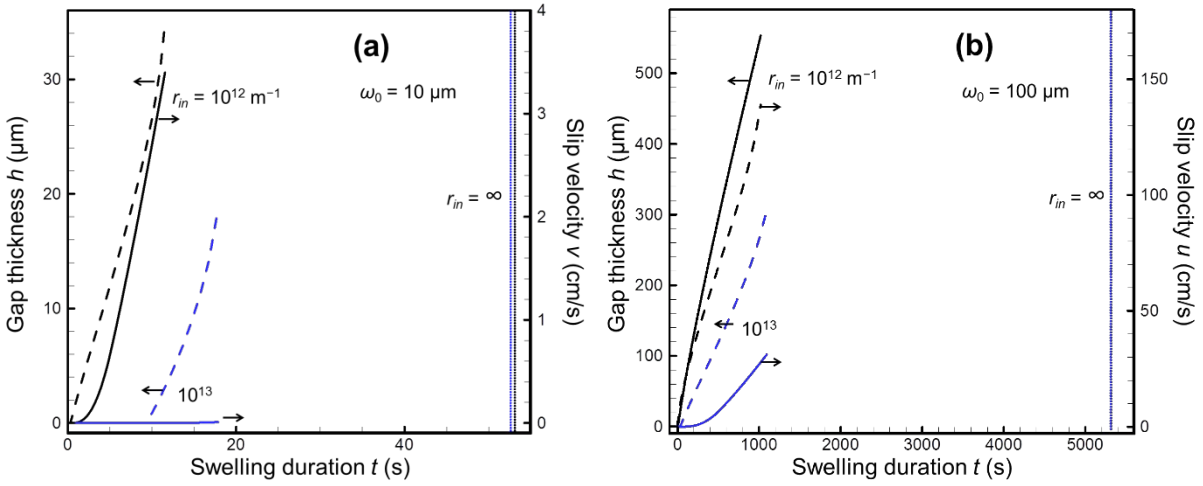

Fig. 9. Estimated values of the gap thickness h (dashed curves) and the tangential velocity of the gel v (solid curves) versus the swelling duration for (a) thin (ω_0 = 10 μm) and (b) thick (ω_0 = 100 μm) filter cakes under the external tangential shear τ_{ext} = 20 Pa. The values of the membrane resistance to filtrate inflow r_{in} are indicated near the curves. The curves end, when the solid gel disappears because of the swelling: $\varphi_{max} = \varphi(\tau_0 = \tau_{ext})$. Horizontals correspond to the moment of the solid gel disappearance in the absence of filtrate inflow across the membrane: $r_{in} = \infty$, $\varphi_m = \varphi(\tau_0 = \tau_{ext})$.

The lower are r_{in} and ω_0, the faster is the gel swelling (Fig. 5a), and the faster is the increasing of h and v with t. In the case of initially thin filter cake (ω_0 = 10 μm, Fig. 9a) the values of h attained before the moment of the solid gel disappearance (final points of the curves in Fig. 9) are of the order of tenth of microns. These low values of h are close to the surface roughness of actual membranes that conflicts with the assumption about the parallel membrane-gel alignment (Fig. 8). It can be speculated that in the case of thin filter cakes, the part of the gel with $\varphi(x) > \varphi(\tau_0 = \tau_{ext})$ can not move along the membrane surface because of the membrane

roughness. Therefore, in this case ω_0 = 10 μm, the swelled cake is swept from the membrane surface only after sufficient swelling duration, when $\varphi(x) < \varphi(\tau_0 = \tau_{ext})$: $t \approx 10$ s at $r_{in} = 10^{12}$ m^{-1} and $t \approx 20$ s at $r_{in} = 10^{13}$ m^{-1}. This noticeably increases the expected time required for complete gel removal from the membrane in the presence of filtrate inflow, from ≈ 1 s to ≈ 10 s at $r_{in} = 10^{12}$ m^{-1} and from ≈ 15 s to ≈ 18 s at $r_{in} = 10^{13}$ m^{-1}. Nevertheless, these values are lower as compared to the time required for the gel swelling in the absence of filtrate inflow across the membrane (≈ 50 s at $r_{in} = \infty$, Fig. 9a), which suggests the positive influence of filtrate inflow on the gel removal. At high filter cake thickness ω_0 = 100 μm, the gel swelling is slow, however, the gap thickness h can reach the values $h > 100$ μm and expected gel tangential velocity can exceed 10 cm·s^{-1} before the gel disappearance (Fig. 9b). Therefore, in the presence of filtrate inflow and absorption by filter cake, an abrupt decrease of residual resistance r_r (Fig. 7a, b) can be also expected in the case of application of non-infinitesimal τ_{ext} for the gel sweeping both for thick and thin filter cakes. This also implies that in the presence of filtrate inflow and absorption across the membrane, the experiment on the swelling-sweeping of thick filter cakes can result in the appearance of gel lumps in the flushing liquid [93, 94] (in contrast to the case with $r_{in} = \infty$, where the membrane is efficiently cleaned, when the gel swelling is completed). Though the swelling duration required for the thick cake sweeping from the surface is too high to have practical application (Fig. 9b), the proposed experiment can be used for the elucidation of the influence of membrane resistance on the filter cake swelling.

Tangential movement ("sliding") of the filter cake, which is discussed above, is different from the apparent wall slip (or wall slip) [95], which is not included in the current simplified model of the filter cake removal. The discussed "sliding" onsets, when the stress applied to the swelling gel exceeds a minimal local value of the true yield stress in the internal swelling part of the gel ($\tau_{ext} > \min(\tau_0)$). The wall slip appears, when τ_{ext} exceeds an apparent local yield stress τ_{0a} ($\tau_{ext} > \tau_{0a}$). For homogeneous yield stress materials with a given particle volume fraction φ, the apparent yield stress is lower that the true one, $\tau_{0a}(\varphi) < \tau_0(\varphi)$ [96]. The value of τ_{0a} is not a material property, it decreases with the increasing of the smoothness on the fixed wall [96]. The information on τ_{0a} is scarce, however, it was reported that for some materials τ_{0a} (as well as τ_0) strongly decreases with decreasing of φ [96]. Hence, the value of τ_{0a} should also decrease during the filter cake swelling on the membrane surface. If the membrane smoothness is not dependent on membrane resistance, the decreasing of τ_{0a} should be faster for the membrane with lower

resistance to filtrate inflow r_{in} because of the faster decreasing of φ in the vicinity of the membrane surface (and φ_m, in particular). Hence, qualitatively, whatever the reason of tangential movement of the swelled filter cake under the external shear stress (wall slip or "sliding"), the decreasing of r_{in} facilitates both (increases the tangential velocity, or decreases τ_{ext} and swelling time required for the onset of tangential movement). The conclusion about easier removal of filter cake in the case of higher membrane permeability and filtrate inflow holds in case of wall slip.

6. Conclusions and final remarks

The model of one-dimensional swelling of colloidal filter cake after the filtration pressure release is developed in the frame of conventional filtration-consolidation theory. The model considers the filter cake as a Terzaghi element, and it takes into account possible filtrate inflow across the membrane under the solid pressure gradient and its uptake by the cake.

The model predicts that the filter cake swelling mechanism and swelling kinetics are determined by the filter cake properties (compressibility, permeability), the initial filter cake resistance r_{ci} and the membrane resistance to filtrate inflow r_{in}. The rate of the cake swelling on the impermeable surface ($r_{in} = \infty$) significantly decreases with increasing of r_{ci} (or initial cake thickness). While in the presence of filtrate inflow across the membrane ($r_{in} \neq \infty$), the swelling rate is less sensitive to r_{ci}, and it increases with decreasing of the membrane resistance to filtrate inflow r_{in}. This is explained by relatively fast filtrate inflow and absorption across the membrane as compared to slower filtrate flow from the bulk suspension throughout the inner part of the filter cake.

At high values of r_{ci}/r_{in} ratio (relatively thick filter cakes on permeable membrane surface), the swelling results in the non-uniform (bell-like) solid concentration distribution in the swelling cake (in contrast to monotonic decreasing of local solid concentration in the cake swelling on an impermeable surface). At a reasonably high initial cake thickness (ω_0 = 100 μm) this prediction can be verified with the help of in situ SAXS-filtration method [74, 83-88].

It is interesting to notice that the positive influence of non-uniform deposit swelling on its removal from non-porous surface is widely discussed, but outside of filtration literature [97-102]. It was demonstrated that formation of more voluminous internal layer under the rigid outer layer of the deposit can result in formation of surface instabilities, which facilitate the deposit detachment. Moreover, an interesting article recently demonstrated that the wrinkles formation

541 during the alginate gel swelling after the reverse osmosis and forward osmosis filtration
542 facilitates the fouling gel detachment and removal from the membrane [103].

543 Further calculations, based on actual rheological properties of colloidal dispersions of
544 casein micelles, show that filtrate inflow across the membrane under the solid pressure gradient
545 can have a noticeable influence on the rate of membrane surface rinsing by external shear force,
546 which is applied after the cake swelling: the decreasing of r_{in} results in the decreasing of the
547 swelling duration required for the filter cake elimination. Because of the bell-like solid
548 concentration distribution in the swelling cake with initially high thickness (ω_0 = 100 μm), it can
549 be swept from the surface under the tangential shear stress, which is lower than the yield stress of
550 the gel. This peculiar dependence of the strength of the filter cake adhesion to the membrane on
551 the swelling duration, the filter cake thickness and the membrane resistance to filtrate inflow can
552 be verified with the help of available methods for analysis of deposit properties [71, 90-92, 104-
553 109].

554 It should be noted that the positive effect of filtrate inflow into the cell (filtrate back
555 permeation) on the membrane surface cleaning is widely demonstrated and modeled in the
556 literature on osmotic backwash or reverse osmosis and forward osmosis membranes (e.g., [110-
557 114]) and hydraulic back pulsing of ultrafiltration membranes (e.g., [115-117]). It is discussed
558 that liquid permeation across the membrane (either under the hydraulic pressure application or
559 the osmotic pressure difference between the filtrate and saline bulk solution) reduces the deposit
560 attachment to the membrane and shifts it away from the membrane surface. This facilitates the
561 deposit removal by tangential flow. The present model results suggest that the same effect
562 (filtrate backflow, gel softening, and its lifting from the membrane surface) can be expected
563 without the hydraulic back-pressure application or increasing the bulk osmotic pressure.

564 A number of assumptions was used in the current model of filter cake swelling: completely
565 reversible cake compression, absence of creep, one-dimensional cake expansion during the
566 swelling, and simplified consideration of cake adhesion to membrane surface and simplified
567 presentation of filtration membrane. Hence, further development of this model can be focused on
568 partial irreversibility of filter cake compression (e.g., as in [44, 45]) and its limited redispersion
569 (as in [20]). It also can include more realistic membrane model (porous surface instead of
570 semipermeable continuum) and account for 2D and 3D swelling (in order to be able to describe
571 possible wrinkles formation [103]).

572 Despite of used assumptions and conclusion that the influence of the membrane resistance
573 to filtrate inflow on the filter cake swelling and removal is less important for thin filter cakes
574 (which are met in membrane filtration applications) as compared to thick filter cakes (that are
575 mainly used for laboratory analysis of filter cakes), we hope that conclusions of current work can
576 be useful in different cases: for example, during the interpretation of experimental data on
577 reversibility of cake formation and compression ([18, 44, 45, 118, 119]), filter cake adhesion to
578 membrane [120], and critical conditions of cake removal from the membrane surface ([21, 94]).
579

Acknowledgments

ML thanks department CEPIA of INRA for the financial support provided for his work in the frame of the project ANS “Emomilé: étude et modélisation de la microfiltration du lait”. The authors thank Dr. Javier Pérez, group leader of the beamline SWING of Synchrotron SOLEIL, for his invaluable help with the project realization. ML equally thanks Dr. Alexander Zaderko for invaluable help with osmotic pressure gedanken experiments.

Appendix A. Analytical solution of basic consolidation equation for cake swelling

Solution of Eq. (7) with conditions (8), (9) and (12) requires the knowledge of pressure dependencies of void ratio $e(p_s)$ and specific filtration resistance $\alpha(p_s)$. In the filtration-consolidation literature it became conventional to replace these dependencies with an effective constant, the modified average consolidation coefficient C_e

$$C_e = \frac{1}{\mu\alpha\rho_s(-\mathrm{d}e/\mathrm{d}p_s)} \tag{A1}$$

which value can quantitatively characterize the kinetics of entire consolidation (or swelling) process for moderately compressible filter cakes. Following the traditional approach and introducing another effective constant, the average specific filtration resistance on the membrane surface α_e, instead of $\alpha_m(p_s)$ into Eq. (12), Eq. (7) can be solved analytically [37, 41, 43, 45, 52], and solid pressure distribution during the swelling can be presented as

$$p_s(\omega,t) = \int_0^1 p_{si}(\xi) \sum_{k=1}^{\infty} \frac{2\lambda_k \sin^2\lambda_k}{\lambda_k - \sin\lambda_k\cos\lambda_k} f_n(\omega) f_n(\xi) \exp\left(-\lambda_k^2 \frac{C_e}{\omega_0^2} t\right) \mathrm{d}\xi \tag{A2}$$

where functions $f_n(\omega)$ and $f_n(\xi)$ are

$$f_n(\omega) = \cos\left(\lambda_k \frac{\omega}{\omega_0}\right) - \cot\lambda_k \sin\left(\lambda_k \frac{\omega}{\omega_0}\right) \tag{A3}$$

$$f_n(\xi) = \cos(\lambda_k\xi) - \cot\lambda_k \sin(\lambda_k\xi) \tag{A4}$$

and λ_k are roots of equation

$$-\frac{\tan\lambda}{\lambda} = \frac{r_{in}}{\rho_s\alpha_e\omega_0} \tag{A5}$$

in the order of increase of their absolute values.

Eq. (A2) is obtained for an arbitrary initial solid pressure distribution in the filter cake $p_{si}(\omega)$. As soon as the current approach is justified only for moderately compressible filter cakes, one can focus only on the linear initial solid pressure distribution:

$$p_{si}(\omega) = p_{mi}(1 - \omega/\omega_0) \tag{A6}$$

where p_{mi} is the initial value of solid pressure at the membrane surface. Introducing Eq. (A6) into (A2) yields

$$p_s(\omega,t) = p_{mi} \sum_{k=1}^{\infty} \frac{2(\sin^2\lambda_k - \lambda_k \sin\lambda_k\cos\lambda_k)}{\lambda_k^2 - \lambda_k \sin\lambda_k\cos\lambda_k} f_n(\omega) \exp\left(-\lambda_k^2 \frac{C_e}{\omega_0^2} t\right) \tag{A7}$$

Using Eq. (A2) the solid pressure at cake-membrane surface ($\omega = 0$) can be determined as

$$p_m(t) = p_{mi} \sum_{k=1}^{\infty} \frac{2(\sin^2 \lambda_k - \lambda_k \sin \lambda_k \cos \lambda_k)}{\lambda_k^2 - \lambda_k \sin \lambda_k \cos \lambda_k} \exp\left(-\lambda_k^2 \frac{C_e}{\omega_0^2} t\right) \quad \text{(A8)}$$

The value of p_m asymptotically approaches 0 during the filter cake swelling. The volume of filtrate absorbed by the swelling filter cake can be obtained with the help of integration of Darcy equation (10) over the swelling time:

$$\frac{V_f(t)}{S} = \frac{p_{mi}}{\mu r_{in}} \frac{\omega_0^2}{C_e} \sum_{k=1}^{\infty} \frac{2}{\lambda_k^2} \cdot \frac{\sin^2 \lambda_k - \lambda_k \sin \lambda_k \cos \lambda_k}{\lambda_k^2 - \lambda_k \sin \lambda_k \cos \lambda_k} \cdot \left[1 - \exp\left(-\lambda_k^2 \frac{C_e}{\omega_0^2} t\right)\right] \quad \text{(A9)}$$

where S is the membrane surface.

The volume of filtrate absorbed by the cake across the membrane increases with time and asymptotically approaches to a certain value $V_{f\infty}$ that is defined as

$$\frac{V_{f\infty}}{S} = \frac{p_{mi}}{\mu r_{in}} \frac{\omega_0^2}{C_e} \sum_{k=1}^{\infty} \frac{2}{\lambda_k^2} \cdot \frac{\sin^2 \lambda_k - \lambda_k \sin \lambda_k \cos \lambda_k}{\lambda_k^2 - \lambda_k \sin \lambda_k \cos \lambda_k} \quad \text{(A10)}$$

The "completeness" of filtrate absorption by the filter cake can be characterized with the help of a ratio U

$$U = \frac{V_f(t)}{V_{f\infty}} \quad \text{(A11)}$$

which changes from 0 to 1 during the filter cake swelling.

Equations analogous to Eqs. (A9) – (A11) are frequently applied for description of different types of consolidation of moderately compressible materials. Therefore, pressure dependencies of $\alpha(p_s)$ and $e(p_s)$ are generally ignored during the modelling: it is assumed that C_e is constant despite the fact that the solid pressure changes with time and across the sample.

The assumption about the constancy of C_e can be acceptable for the cases where the average solid pressure, that governs the process, does not change significantly with time: for example, during mechanical compression with small pressure increments.

However, in contrast to different consolidation processes, description of a filter cake swelling on a membrane surface requires an additional parameter, the average specific filtration resistance α_e of the filter cake layer adjacent to the membrane surface (parameter α_e appears in Eq. (A2) and following equations via Eq. (A5)). It substitutes an actual pressure dependency $\alpha(p_m)$, where p_m is the solid pressure on the cake-membrane surface. The latter decreases from p_{mi} to 0 (Eq. (A8)), which implies significant decrease of α during the swelling. In the present paper devoted to the role of membrane resistance in the filter cake swelling, this decrease can not be

ignored, because, in accordance to Eq. (A5), the value of specific filtration resistance α on the membrane surface is of the same importance for description of cake swelling as the value of the membrane resistance r_{in}.

Therefore, numerical solution of Eq. (7) was preferred in the current paper in order to avoid the ambiguities concerning the role of membrane resistance in cake swelling.

Nevertheless, it was observed that same trends are predicted for the solid pressure evolution with the help of numerical solution of Eq. (7) and with application of Eqs. (A2) – (A11).

Appendix B. Basic consolidation equation for cake swelling, numerical solution

The dependencies of osmotic pressure (solid pressure) $p_s(c)$ and hydraulic permeability $\kappa(c)$ and on the mass concentration of solid c reported by Bouchoux et al. [121] for aqueous dispersions of casein micelles were used in numerical solution of Eq. (7):

$$p_s(c) = 8c + b_p c^2 + c_p c^2 + f_p c^6 \tag{B1}$$

$$\kappa(c) = (a_\kappa c + b_\kappa c^2 + f_\kappa c^6)^{-1} \tag{B2}$$

Here c is expressed in kg/m^3, and numerical values of polynomial coefficients are a_p = 8, b_p = $3\cdot10^{-2}$, c_p = 10^{-5}, f_p = $3\cdot10^{-11}$, a_κ = $9.2\cdot10^{14}$, b_κ = $1.1\cdot10^{12}$, f_κ = $4.6\cdot10^{3}$. These dependencies are discussed in Appendix C.

Introducing the dependencies $\kappa(c)$ and $p_s(c)$ into Eq. (7) with the help of relations (C1) – (C2) and the definition of the void ratio

$$e = (1-\varphi)/\varphi \tag{B3}$$

yield handy forms of basic consolidation equation

$$\frac{\partial c}{\partial t} = \frac{c^2}{\mu\rho_s^2}\cdot\frac{\partial}{\partial\omega}\left(c\,\kappa(c)\frac{\partial\, p_s(c)}{\partial c}\cdot\frac{\partial c}{\partial\omega}\right) \tag{B4}$$

as well as initial and boundary conditions. When the swelling is preceded by the constant pressure dead-end filtration that results in formation of a filter cake with the solid concentration distributed from c_{mi} (on the membrane surface where ω = 0) to c_0 (on the cake-suspension interface where $\omega = \omega_0$), the initial condition (8) can be rewritten as

$$\int_{c}^{c_{mi}} c\,\kappa(c)\frac{\partial\, p_s(c)}{\partial c}\,\mathrm{d}c = \frac{\omega}{\omega_0}\int_{c_0}^{c_{mi}} c\,\kappa(c)\frac{\partial\, p_s(c)}{\partial c}\,\mathrm{d}c \qquad \text{at } t = 0 \tag{B5}$$

The boundary conditions (9) and (12) can be represented as

$$c = c_0 \qquad \text{at } \omega = \omega_0 \tag{B6}$$

$$\frac{\mathrm{d}c}{\mathrm{d}\omega} = \frac{p_s(c)}{r_{in}} \cdot \frac{\rho_s}{c\,\kappa(c)\dfrac{\partial\, p_s(c)}{\partial c}} \qquad \text{at } \omega = 0 \tag{B7}$$

Eq. (B4) can be solved with initial and boundary conditions (B5) – (B7) for known dependencies κ(c) and $p_s(c)$ and given values of parameters r_{in}, c_{mi} and ω_0. The initial solid concentration on the cake-membrane interface of c_{mi} (in Eq. (B5)) is defined by the pressure applied during the cake formation (i.e., dead-end filtration) ΔP and the ratio of inside-out membrane resistance r_m to the filter cake resistance attained at the end of filtration r_{ci} as

$$p_s(c_{mi}) = \Delta P/(1 + r_m/r_{ci}) \tag{B8}$$

where r_{ci} is defined from

$$r_{ci} = \rho_s \omega_0 \cdot \frac{p_s(c_{mi})}{\int_{c_0}^{c_{mi}} c\,\kappa(c)\dfrac{\partial\, p_s(c)}{\partial c}\,\mathrm{d}c} \tag{B9}$$

Eq. (7) was solved (dependencies $c(\omega/\omega_0, t)$ were obtained) by the Crank-Nicholson method with the help of Maple 18 (Maplesoft). Temporal and spatial step sizes were chosen such that their reduction would have had no observable effect on the result of calculation of local properties (compressibility, permeability, and further tangential velocity) of the swelling cake.

In order to study the influence of the possibility and intensity of filtrate inflow across the membrane on the filter cake swelling, Eq. (7) was solved for different values of r_{in}, including the case $r_{in} = \infty$, which corresponds to the absence of filtrate absorption by the cake. The value of ω_0, used for solution, was varied from 10 to 200 μm. Particular attention was focused on the cases $\omega_0 = 10$ μm and $\omega_0 = 100$ μm. The former corresponds to "thin" filter cakes, which can be met in membrane filtration applications, while the latter simulates rather "thick" filter cakes (or deposits) that are usually obtained in laboratory studies on filtration and/or surface cleaning [74, 83-88, 90-92]. Other parameters were fixed at reasonable values: the pressure applied during the cake formation $\Delta P = 10^5$ Pa, the filtrate viscosity $\mu = 10^{-3}$ Pa·s, the bulk concentration of casein micelles dispersion $\varphi_0 = 0.02$.

Appendix C. Casein micelles dispersions, material properties

Casein micelles, which properties are used in order to describe colloids typically met in filtration, are well characterized natural spherical porous colloidal particles, highly compressible and deformable, stable against the aggregation at neutral pH [122]. Using the methods of osmotic

stress and dead-end filtration, Bouchoux et al. obtained dependencies of hydraulic permeability κ and osmotic pressure of casein micelles dispersions on the solids concentration c for a wide range of solid pressure [121]. These dependencies are presented by Eqs. (B1) – (B2). The osmotic pressure of casein micelles dispersions attained in osmotic stress experiments is equivalent to their compressive pressure (solid pressure). The specific filtration resistance and the solids volume fraction can be obtained from the data of Bouchoux et al. [121] as

$$\alpha = 1/\kappa c \tag{C1}$$

$$\varphi = c/\rho_s \tag{C2}$$

The density of solids of casein micelles can be calculated from the values of micelles voluminosity and the micelles density reported by de Kruif and Huppertz [123]: ρ_s = 1.35 g/ml (which is close to the value provided by Morris et al. [124]). The obtained dependencies $\alpha(p_s)$ and $\varphi(p_s)$ presented in Fig. C1.

Fig. C1.

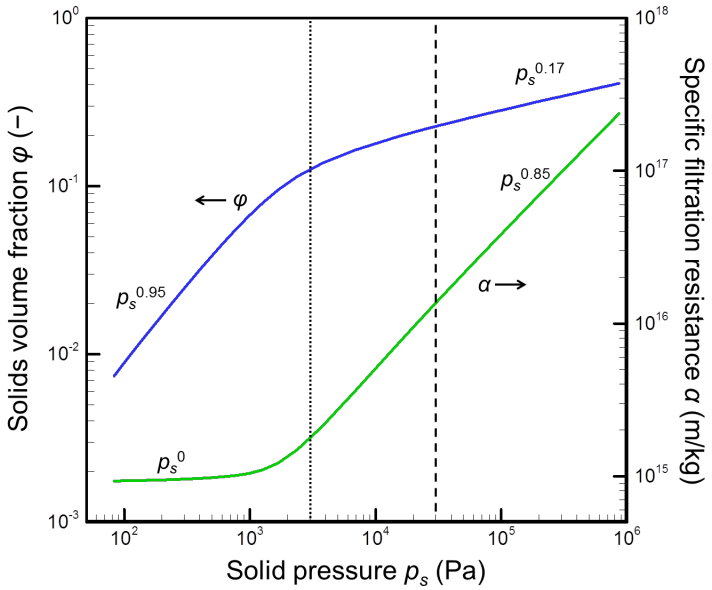

Fig. C1. Pressure dependency of solids volume fraction and specific filtration resistance for aqueous dispersions of casein micelles (calculated from the data reposted by Bouchoux et al. [121]). Dotted vertical corresponds to the solid pressure in the point of sol-gel transition; dashed vertical corresponds to the solid pressure required for "irreversible" gel formation.

At low particle concentration, casein micelles dispersions are sols with practically linear dependence between solids volume fraction and solid pressure and practically constant and low specific filtration resistance. According to the data of Bouchoux et al. [125, 126], the point of fluid sol to solid gel transition of casein micelles dispersions corresponds to the solid pressure about $p_s \approx 3$ kPa. Further, the increase of solid pressure above 30 kPa results into the "irreversible" gel formation; that is determined from the dead-end ultrafiltration experiments [19]). As well as many colloidal filter cakes, at high solid pressure, casein micelles gels have moderate compressibility ($\varphi \propto p_s^{0.17}$) and high specific filtration resistance that strongly depends on p_s ($\alpha = 10^{16}\ldots10^{17}$ m/kg, $\alpha \propto p_s^{0.95}$).

According to Jin et al. [83], for a wide range of solid volume fraction $\varphi = 0.02 - 0.147$ rheological properties of aqueous dispersions of casein micelles can be described by Herschel-Bulkley model

$$\tau = \tau_0 + K\dot{\gamma}^N \tag{C3}$$

where τ is the shear stress, $\dot{\gamma}$ is the shear rate, and K, N and τ_0 (yield stress) are parameters that depend on the solid volume fraction. Figure C2 presents these dependencies obtained via the least-square fitting of experimental $\tau(\dot{\gamma})$ data reported by Jin et al. [83] for different casein micelles concentrations.

Fig. C2.

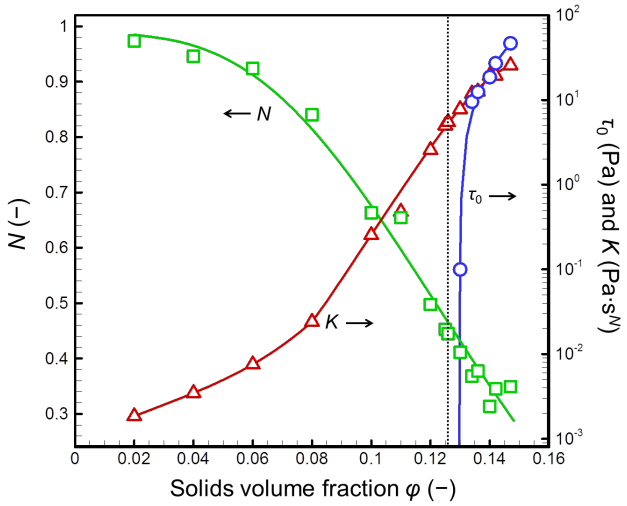

Fig. C2. Values of parameters of Herschel-Bulkley model for casein micelles dispersions at

different solid concentrations: symbols – data obtained by least-square fitting of experimental dependencies $\tau(\dot{\gamma}, \varphi)$ (presented by Jin at al. [83]) with the help of Eq. (C3), curves – result of best curve fitting for these data. Dotted vertical corresponds to the concentration of sol-gel transition.

Though dependencies presented in Figs. C1 – C2 were obtained either for equilibrium dispersions (prepared via powder rehydration or osmotic concentration), or dynamically compressed filter cakes (during the dead-end filtration), it was assumed that they are valid for description of local properties of filter cakes during the swelling.

References

[1] P. Bacchin, P. Aimar, V. Sanchez. Model for colloidal fouling of membranes. AIChE Journal, 41 (1995) 368-376.

[2] P. Harmant, P. Aimar. Coagulation of colloids retained by porous wall. AIChE Journal, 42 (1996) 3523-3532.

[3] P. Bacchin, D. Si-Hassen, V. Starov, M. J. Clifton, P. Aimar. A unifying model for concentration polarization, gel-layer formation and particle deposition in cross-flow membrane filtration of colloidal suspensions. Chemical Engineering Science, 57 (2002) 77-91.

[4] P. Aimar, P. Bacchin. Slow colloidal aggregation and membrane fouling. Journal of Membrane Science, 360 (2010) 70-76.

[5] Y. K. Benkahla, A. Ould-Dris, M. Y. Jaffrin, D. Si-Hassen. Cake growth mechanism in cross-flow microfiltration of mineral suspensions. Journal of Membrane Science, 98 (1995) 107-117.

[6] L. Defrance, M. Y. Jaffrin. Reversibility of fouling formed in activated sludge filtration. Journal of Membrane Science, 157 (1999) 73-84.

[7] G. Gesan-Guiziou, G. Daufin, E. Boyaval. Critical stability conditions in skimmed milk crossflow microfiltration: Impact on operating modes. Lait, 80 (2000) 129-138.

[8] A. S. Grandison, W. Youravong, M. J. Lewis. Hydrodynamic factors affecting flux and fouling during ultrafiltration of skimmed milk. Lait, 80 (2000) 165-174.

[9] B. Espinasse, P. Bacchin, P. Aimar. On an experimental method to measure critical flux in ultrafiltration. Desalination, 146 (2002) 91-96.

[10] W. Youravong, M. J. Lewis, A. S. Grandison. Critical flux in ultrafiltration of skimmed milk. Food and Bioproducts Processing: Transactions of the Institution of Chemical Engineers, Part C, 81 (2003) 303-308.

[11] G. Gesan-Guiziou, A. Jimenez, C. Arcelin. Cake properties in dead-end ultrafiltration of casein micelles: determination of critical operating conditions. Desalination, 199 (2006) 20-22.

[12] K. Nakanishi, H.-G. Kessler. Rinsing behavior of deposited layers formed on membranes in ultrafiltration. Journal of Food Science, 50 (1985) 1726-1731.

[13] H. C. Chua, T. C. Arnot, J. A. Howell. Controlling fouling in membrane bioreactors operated with a variable throughput. Desalination, 149 (2002) 225-229.

[14] P. van der Marel, A. Zwijnenburg, A. Kemperman, M. Wessling, H. Temmink, W. van der Meer. An improved flux-step method to determine the critical flux and the critical flux for irreversibility in a membrane bioreactor. Journal of Membrane Science, 332 (2009) 24-29.

[15] J. Ma, Z. Wang, Z. Wu, Q. Wang. An improved step-wise method to determine critical flux of membrane bioreactor by adding relaxation zone. Journal of Tongji University, 39 (2011) 1663-1668.

[16] M. K. Jorgensen, K. Keiding, M. L. Christensen. On the reversibility of cake buildup and compression in a membrane bioreactor. Journal of Membrane Science, 455 (2014) 152-161.

[17] W. Zhang, L. Ding, M. Y. Jaffrin, B. Tang. Membrane cleaning assisted by high shear stress for restoring ultrafiltration membranes fouled by dairy wastewater. Chemical Engineering Journal, 325 (2017) 457-465.

[18] M. K. Jorgensen, B. H. Hede, M. L. Christensen. Modeling approach to describe fouling removal during relaxation. Journal of the Taiwan Institute of Chemical Engineers, 94 (2019) 119-123.

[19] P. Qu, G. Gesan-Guiziou, A. Bouchoux. Dead-end filtration of sponge-like colloids: The case of casein micelle. Journal of Membrane Science, 417-418 (2012) 10-19.

[20] P. Qu, G. Gesan-Guiziou, A. Bouchoux. On the cohesive properties of casein micelles in dense systems. Food Hydrocolloids, 43 (2015) 753-762.

[21] T. Steinhauer, J. Lonfat, I. Hager, R. Gebhardt, U. Kulozik. Effect of pH, transmembrane pressure and whey proteins on the properties of casein micelle deposit layers. Journal of Membrane Science, 493 (2015) 452-459.

[22] D. E. Rosner. Lifetime of a highly soluble dense spherical particle. Journal of Physical Chemistry, 73 (1969) 382-387.

[23] P. I. Lee, N. A. Peppas. Prediction of polymer dissolution in swellable controlled-release systems. Journal of Controlled Release, 6 (1987) 207-215.

[24] H.-R. Lee, Y.-D. Lee. Mathematical models and experiments for swelling phenomena before dissolution of a polymer film. Chemical Engineering Science, 46 (1991) 1771-1779.

[25] E. S. Mickaily, S. Middleman. Hydrodynamic cleaning of a viscous film from the inside of a long tube. AIChE Journal, 39 (1993) 885-893.

[26] I. Devotta, V. D. Ambeskar, A. B. Mandhare, R. A. Mashelkar. The life time of a dissolving polymeric particle. Chemical Engineering Science, 49 (1994) 645-654.

771 [27] V. V. Ranade, R. A. Mashelkar. Convective diffusion from a dissolving polymeric particle.
772 AIChE Journal, 41 (1995) 666-676.
773 [28] C. R. Gillham, P. J. Fryer, A. P. M. Hasting, D. I. Wilson. Cleaning-in-place of whey protein
774 fouling deposits: Mechanisms controlling cleaning. Food and Bioproducts Processing:
775 Transactions of the Institution of Chemical Engineers, Part C, 77 (1999) 127-136.
776 [29] M. J. Davey, K. A. Landman, M. J. McGuinness, H. N. Jin. Mathematical modeling of rice
777 cooking and dissolution in beer production. AIChE Journal, 48 (2002) 1811-1826.
778 [30] H. Xin, X. D. Chen, N. Ozkan. Cleaning rate in the uniform cleaning stage for whey protein
779 gel deposits. Food and Bioproducts Processing: Transactions of the Institution of of Chemical
780 Engineers, Part C, 80 (2002) 240-246.
781 [31] W.-M. Lu, K.-L. Tung, C.-H. Pan, K.-J. Hwang. Crossflow microfiltration of mono-
782 dispersed deformable particle suspension. Journal of Membrane Science, 198 (2002) 225-243.
783 [32] H. Xin, X. D. Chen, N. Ozkan. Removal of a model protein foulant from metal surfaces.
784 AIChE Journal, 50 (2004) 1961-1973.
785 [33] P. E. Bouquerand, S. Maio, V. Normand, S. Singleton, D. Atkins. Swelling and erosion
786 affecting flavor release from glassy particles in water. AIChE Journal, 50 (2004) 3257-3270.
787 [34] E. Kaunisto, M. Marucci, P. Borgquist, A. Axelsson. Mechanistic modelling of drug release
788 from polymer-coated and swelling and dissolving polymer matrix systems. International Journal
789 of Pharmaceutics, 418 (2011) 54-77.
790 [35] P. Valois, E. Verneuil, F. Lequeux, L. Talini. Understanding the role of molar mass and
791 stirring in polymer dissolution. Soft Matter, 12 (2016) 8143-8154.
792 [36] A. Briffaz, P. Bohuon, J. M. Meot, B. Matignon-Pons, C. Mestres. Modelling of water
793 transport with convection effects on amylose transfer in a swelling, eroding and gelatinizing
794 starchy matrix. Journal of Food Engineering, 221 (2018) 132-140.
795 [37] T. Murase, M. Iwata, M. Wakita, T. Adachi, N. Hayashi, M. Shirato. Expansion of
796 consolidated material after release of load. Journal of Chemical Engineering of Japan, 22 (1989)
797 195-199.
798 [38] T. Murase, M. Iwata, T. Adachi, M. Wakita. Stress relaxation of expressed cake. Journal of
799 Chemical Engineering of Japan, 22 (1989) 655-659.
800 [39] T. Murase, M. Iwata, T. Adachi. Expansion of inhomogeneous cake after release of load.
801 Journal of Chemical Engineering of Japan, 23 (1990) 108-110.

802 [40] M. Shirato, T. Murase, E. Iritani, S. Nakatsuka. Experimental analysis of flux decline
803 mechanism of batch ultrafiltration (filtration characteristics of gel layer). Filtration and
804 Separation, 28 (1991) 104-109.
805 [41] M. Iwata, T. Murase. Expansion and stress relaxation of expressed cake. Drying
806 Technology, 11 (1993) 749-767.
807 [42] M. Iwata, S. Koda, H. Nomura. Theory of compression and expansion of hydrogels. Journal
808 of Chemical Engineering of Japan, 32 (1999) 684-688.
809 [43] E. Iritani, N. Katagiri, K.-M. Yoo, H. Hayashi. Consolidation and expansion of a granular
810 bed of superabsorbent hydrogels. AIChE Journal, 53 (2007) 129-137.
811 [44] E. Iritani, N. Katagiri, G. Inagaki. Compression and expansion properties of filter cake
812 accompanied with step change in applied pressure in membrane filtration. Separation and
813 Purification Technology, 198 (2018) 3-9.
814 [45] E. Iritani, N. Katagiri, T. Yoshida. Simplified evaluation of consolidation and expansion
815 behaviour of highly compressible cake. Filtration, 18 (2018) 50-60.
816 [46] P. J. Banks. Theory of constant-rate expression and subsequent relaxation. Proceedings of
817 the 4th International Drying Symposium (IDS), 1984, Kyoto, Japan.
818 [47] J. Olivier, J. Vaxelaire, E. Vorobiev. Modelling of cake filtration: An overview. Separation
819 Science and Technology, 42 (2007) 1667-1700.
820 [48] D. J. Lee, C. H. Wang. Theories of cake filtration and consolidation and implications to
821 sludge dewatering. Water Research, 34 (2000) 1-20.
822 [49] F. M. Tiller, C. S. Yeh. The role of porosity in filtration. Part XI: Filtration followed by
823 expression. AIChE Journal, 33 (1987) 1241-1256.
824 [50] M. Elimelech, S. Bhattacharjee. A novel approach for modeling concentration polarization
825 in crossflow membrane filtration based on the equivalence of osmotic pressure model and
826 filtration theory. Journal of Membrane Science, 145 (1998) 223-241.
827 [51] E. Iritani, N. Katagiri, M. Tsukamoto, K.-J. Hwang. Determination of cake properties in
828 ultrafiltration of nano-colloids based on single step-up pressure filtration test. AIChE Journal, 60
829 (2014) 289-299.
830 [52] M. Iwata, M. S. Jami. Theoretical analysis of centrifugal dewatering of superabsorbent
831 hydrogels using Terzaghi-Voigt combined model. European Polymer Journal, 43 (2007) 5026-
832 5033.

[53] T. Tanaka, D. J. Fillmore. Kinetics of swelling of gels. The Journal of Chemical Physics, 70 (1979) 1214-1218.

[54] M. Shirato, T. Murase, N. Hayashi, T. Fukushima. Constant pressure expression of solid-liquid mixtures with medium resistance. Journal of Chemical Engineering of Japan, 10 (1977) 154-159.

[55] C. Tien. Principles of filtration. Elsevier, Oxford, 2013.

[56] T. Murase, H. Moridera, M. Negawa, M. Shirato. Analysis of expression operations. Journal of Chemical Engineering of Japan, 4 (1971) 263-268.

[57] J.-J. Qin, B. Liberman, K. A. Kekre. Direct osmosis for reverse osmosis fouling control: Principles, applications and recent developments. Open Chemical Engineering Journal, 3 (2009) 8-16.

[58] E. Vorobiev. Derivation of filtration equations incorporating the effect of pressure redistribution on the cake-medium interface: A constant pressure filtration. Chemical Engineering Science, 61 (2006) 3686-3697.

[59] E. Iritani, N. Katagiri, Y. Takaishi, S. Kanetake. Determination of pressure dependence of permeability characteristics from single constant pressure filtration test. Journal of Chemical Engineering of Japan, 44 (2011) 14-23.

[60] E. Iritani, N. Katagiri, S. Kanetake. Determination of cake filtration characteristics of dilute suspension of bentonite from various filtration tests. Separation and Purification Technology, 92 (2012) 143-151.

[61] E. Iritani, N. Katagiri, H. Masuda. Evaluation of variable pressure dead-end ultrafiltration behaviors of nanocolloids based on filter cake properties. Chemical Engineering Research and Design, 134 (2018) 528-539.

[62] H. Soodak, A. Iberall. Forum on osmosis. IV. More on osmosis and diffusion. American Journal of Physiology - Regulatory Integrative and Comparative Physiology, 6 (1979) R114-R122.

[63] H. R. Hirsch. Negative solvent pressure in osmosis: A Gedanken experiment. Journal of Biological Physics, 8 (1980) 11-17.

[64] Ph. C. Nelson. Biological physics: energy, information, life. W. H. Freeman and Co, New York, 2008 (p. 257).

[65] A. Mauro. Osmotic flow in a rigid porous membrane. Science, 149 (1965) 867-869.

[66] K. Terzaghi. Theoretical soil mechanics. John Wiley & Sons, Inc., New York, 1943 (p. 330).
[67] N. Gao, J. Wang, L. Song. Independence of hydraulic pressures on the feed and draw solutions in the osmotically driven membrane processes. Journal of Membrane Science, 586 (2019) 1-6.
[68] H. Zhang, J. Wang, K. Rainwater, L. Song. Metastable state of water and performance of osmotically driven membrane processes. Membranes, 9 (2019) 43.
[69] R. M. Pashley, M. J. Francis, M. Rzechowicz. Unusual properties of water: Effects on desalination processes. Water, 35 (2008) 67-71.
[70] Y. Gao, S. Haavisto, W. Li, C. Y. Tang, J. Salmela, A. F. Fane. Novel approach to characterizing the growth of a fouling layer during membrane filtration via optical coherence tomography. Environmental Science and Technology, 48 (2014) 14273-14281.
[71] P. W. Gordon, M. Scholer, H. Foste, M. Helbig, W. Augustin, Y. M. John Chew, S. Scholl, J.-P. Majschak, D. I. Wilson. A comparison of local phosphorescence detection and fluid dynamic gauging methods for studying the removal of cohesive fouling layers: Effect of layer roughness. Food and Bioproducts Processing, 92 (2014) 46-53.
[72] C. Gaucher, P. Jaouen, J. Comiti, P. Legentilhomme. Determination of cake thickness and porosity during cross-flow ultrafiltration on a plane ceramic membrane surface using an electrochemical method. Journal of Membrane Science, 210 (2002) 245-258.
[73] C. Gaucher, P. Legentilhomme, P. Jaouen, J. Comiti, J. Pruvost. Hydrodynamics study in a plane ultrafiltration module using an electrochemical method and particle image velocimetry visualization. Experiments in Fluids, 32 (2002) 283-293.
[74] C. Rey, N. Hengl, S. Baup, M. Karrouch, A. Dufresne, H. Djeridi, R. Dattani, F. Pignon. Velocity, stress and concentration fields revealed by micro-PIV and SAXS within concentration polarization layers during cross-flow ultrafiltration of colloidal Laponite suspensions. Journal of Membrane Science, 578 (2019) 69-84.
[75] M. Gholami, A. Rashedi, N. Lenoir, D. Hautemayou, G. Ovarlez, S. Hormozi. Time-resolved 2D concentration maps in flowing suspensions using X-ray. Journal of Rheology, 62 (2018) 955-974.
[76] F. Arndt, S. Schuhmann, G. Guthausen, S. Schutz, H. Nirschl. In situ MRI of alginate fouling and flow in ceramic hollow fiber membranes. Journal of Membrane Science, 524 (2017) 691-699.

[77] F. Arndt, U. Roth, H. Nirschl, S. Sc hutz, G. Guthausen. New insights into sodium alginate fouling of ceramic hollow fiber membranes by NMR imaging. AIChE Journal, 62 (2016) 2459-2467.

[78] N. Schork, S. Schuhmann, F. Arndt, S. Schutz, G. Guthausen, H. Nirschl. MRI investigations of filtration: Fouling and cleaning processes , Microporous and Mesoporous Materials, 269 (2018) 60-64.

[79] N. Collier, P. Debreyne, G. Delaplace, B. Chen, D. Callens, P. Campistron, B. Nongaillard. Contribution of the shear wave ultrasonic reflectometry to the stickiness measurements. Ultrasonics, 89 (2018) 187-194.

[80] K.-L. Tung, S. Wang, W.-M. Lu, C.-H. Pan. In situ measurement of cake thickness distribution by a photointerrupt sensor. Journal of Membrane Science, 190 (2011) 57-67.

[81] Monitoring and visualizing membrane-based processes. Eds. C. Guell, M. Ferrando, F. Lopez. Wiley, 2009.

[82] V. Chen, H. Li, A. G. Fane. Non-invasive observation of synthetic membrane processes - A review of methods. Journal of Membrane Science, 241 (2004) 23-44.

[83] Y. Jin, N. Hengl, S. Baup, F. Pignon, N. Gondrexon, M. Sztucki, G. Gesan-Guiziou, A. Magnin, M. Abyan, M. Karrouch, D. Bleses. Effects of ultrasound on cross-flow ultrafiltration of skim milk: characterization from macro-scale to nano-scale. Journal of Membrane Science, 470 (2014) 205-218.

[84] C. David, F. Pignon, T. Narayanan, M. Sztucki, G. Gesan-Guiziou, A. Magnin. Spatial and temporal in situ evolution of the concentration profile during casein micelle ultrafiltration probed by small-angle X-ray scattering. Langmuir, 24 (2008) 4523-4529.

[85] F. Pignon, G. Belina, T. Narayanan, X. Paubel, A. Magnin, G. Gesan-Guiziou. Structure and rheological behavior of casein micelle suspensions during ultrafiltration process. Journal of Chemical Physics, 121 (2004) 8138-8146.

[86] F. Doudiès, M. Loginov, F. Lambrouin, N. Leconte, L. Sharpnack, F. Pignon, G. Gesan-Guiziou. Structural organization of casein micelles in concentrated layer during cross-flow ultrafiltration. Proceedings of the conference Fouling and Cleaning in Food Processing, 2018, Lund, Sweden.

[87] F. Doudiès, M. Loginov, F. Garnier-Lambrouin, N. Leconte, L. Sharpnack, N. Hengl, F. Pignon, G. Gesan-Guiziou. Understanding of casein micelles concentrated layers properties

926 during cross flow ultrafiltration by in-situ small-angle X-ray scattering (SAXS). Proceedings of
927 the Euromembrane 2018 conference, 2018, Valencia, Spain.
928 [88] F. Doudiès, M. Loginov, N. Hengl, F. Pignon, N. Leconte, F. Garnier-Lambrouin, J. Perez,
929 M. Granger-Delacroix, M. Belna, G. Gesan-Guiziou. Small-Angle X-Ray Scattering (SAXS)
930 analyses of build-up, relaxation and erosion of casein micelles fouling layer during cross-flow
931 ultrafiltration. Proceedings of the European Conference on Fluid-Particle Separation FPS2018,
932 2018, Lyon, France.
933 [89] J. Crank. The mathematics of diffusion. London, Oxford University Press, 1975.
934 [90] T. Mattsson, W. J. T. Lewis, Y. M. J. Chew, M. R. Bird. In situ investigation of soft cake
935 fouling layers using fluid dynamic gauging. Food and Bioproducts Processing, 93 (2015) 205-
936 210.
937 [91] W. J. T. Lewis, T. Mattsson, Y. M. J. Chew, M. R. Bird. Investigation of cake fouling and
938 pore blocking phenomena using fluid dynamic gauging and critical flux models. Journal of
939 Membrane Science, 533 (2017) 38-47.
940 [92] T. Mattsson, W. J. T. Lewis, Y. M. J. Chew, M. R. Bird. The use of fluid dynamic gauging
941 in investigating the thickness and cohesive strength of cake fouling layers formed during cross-
942 flow microfiltration. Separation and Purification Technology, 198 (2018) 25-30.
943 [93] A. J. E. Jimenez-Lopez, N. Leconte, O. Dehainault, C. Geneste, L. Fromont, G. Gesan-
944 Guiziou. Role of milk constituents on critical conditions and deposit structure in skimmilk
945 microfiltration (0.1 μm). Separation and Purification Technology, 61 (2008) 33-43.
946 [94] N. Wemsy Diagne, M. Rabiller-Baudry, M., L. Paugam. On the actual cleanability of
947 polyethersulfone membrane fouled by proteins at critical or limiting flux. Journal of Membrane
948 Science, 425-426 (2013) 40-47.
949 [95] D. Bonn, M. M. Denn, L. Berthier, T. Divoux, S. Manneville. Yield stress materials in soft
950 condensed matter. Reviews of Modern Physics, 89 (2017) 035005.
951 [96] J. R. Seth, M. Cloitre, R. T. Bonnecaze. Influence of short-range forces on wall-slip in
952 microgel pastes. Journal of Rheology, 52 (2008) 1241-1268.
953 [97] K. T. Tan, B. D. Vogt, C. C. White, K. L. Steffens, J. Goldman, S. K. Satija, C. Clerici, D.
954 L. Hunston. On the origins of sudden adhesion loss at a critical relative humidity: Examination of
955 bulk and interfacial contributions. Langmuir, 24 (2008) 9189-9193.

956 [98] B. Jing, J. Zhao, Y. Wang, X. Yi, H. Duan. Water-swelling-induced morphological
957 instability of a supported polymethyl methacrylate thin film. Langmuir, 26 (2010) 7651-7655.
958 [99] S. Yang, K. Khare, P.-C. Lin. Harnessing surface wrinkle patterns in soft matter. Advanced
959 Functional Materials, 20 (2010) 2550-2564.
960 [100] R. P. Berkelaar, P. Bampoulis, E. Dietrich, H. P. Jansen, X. Zhang, E. S. Kooij, D. Lohse,
961 H. J. W. Zandvliet. Water-induced blister formation in a thin film polymer. Langmuir, 31 (2015)
962 1017-1025.
963 [101] C. White, K. T. Tan, D. Hunston, K. Steffens, D. L. Stanley, S. K. SAtija, B. Akgun, B. D.
964 Vogt. Mechanisms of criticality in environmental adhesion loss. Soft Matter, 11 (2015) 3994-
965 4001.
966 [102] Q. Wang, X. Zhao. A three-dimensional phase diagram of growth-induced surface
967 instabilities. Scientific Reports, 5 (2015) 8887 (1-9).
968 [103] E. W. Tow, M. M. Rencken, J. H. Lienhard. In situ visualization of organic fouling and
969 cleaning mechanisms in reverse osmosis and forward osmosis. Desalination, 399 (2016) 138-147.
970 [104] R. J. Hooper, W. Liu, P. J. Fryer, W. R. Paterson, D. I. Wilson, Z. Zhang. Comparative
971 studies of fluid dynamic gauging and a micromanipulation probe for strength measurements.
972 Food and Bioproducts Processing, 84 (2006) 353-358.
973 [105] W. Liu, G. K. Christian, Z. Zhang, P. J. Fryer. Direct measurement of the force required to
974 disrupt and remove fouling deposits of whey protein concentrate. International Dairy Journal, 16
975 (2006) 164-172.
976 [106] P. W. Gordon, A. D. M. Brooker, Y. M. J. Chew, D. I. Wilson, D. W. York. Studies into
977 the swelling of gelatine films using a scanning fluid dynamic gauge. Food and Bioproducts
978 Processing, 88 (2010) 357-364;
979 [107] P. Saikhwan, R. Mercade-Prieto, Y. M. J. Chew, S. Gunasekaran, W. R. Paterson, D. I.
980 Wilson. Swelling and dissolution in cleaning of whey protein gels. Food and Bioproducts
981 Processing, 88 (2010) 375-383.
982 [108] N. Akhtar, J. Bowen, K. Asteriadou, P. T. Robins, Z. Zhang, P. J. Fryer. Matching the
983 nano- to the meso-scale: Measuring deposit-surface interactions with atomic force microscopy
984 and micromanipulation. Food and Bioproducts Processing, 88 (2010) 341-348.

985 [109] A. Ali, D. De'Ath, D. Gibson, J. Parkin, G. Ward, D. I. Wilson. Development of a
986 “millimanipulation” device to study the removal of soft solid fouling layers from solid substrates
987 and its application to cooked lard deposits. Food and Bioproducts Processing, 93 (2015) 256-268.
988 [110] A. Sagiv, R. Semiat. Modeling of backwash cleaning methods for RO membranes.
989 Desalination, 261 (2010) 338-346.
990 [111] C. Kim, S. Lee, S. Hong. Application of osmotic backwashing in forward osmosis:
991 Mechanisms and factors involved. Desalination and Water Treatment, 43 (2012) 314-322.
992 [112] M. M. Motsa, B. B. Mamba, A. D'Haese, E. M. V. Hoek, A. R. D. Hoek. Organic fouling
993 in forward osmosis membranes: The role of feed solution chemistry and membrane structural
994 properties. Journal of Membrane Science, 460 (2014) 99-109.
995 [113] G. Blandin, H. Vervoort, P. Le-Clech, A. R. D. Verliefde. Fouling and cleaning of high
996 permeability forward osmosis membranes. Journal of Water Process Engineering, 9 (2016) 161-
997 169.
998 [114] M. M. Motsa, B. B. Mamba, J. M. Thwala, A. R. D. Verliefde. Osmotic backwash of
999 fouled FO membranes: Cleaning mechanisms and membrane surface properties after cleaning.
1000 Desalination, 402 (2017) 62-71.
1001 [115] R. K. Lalrinsanga, N. B. Bejgam, S. Ganguly. Effect of pressure pulsing on concentration
1002 boundary layer over membrane – A numerical investigation. Asia-Pacific Journal of Chemical
1003 Engineering, 8 (2013) 519-526.
1004 [116] F. Vinther, M. Pinelo, M. Brons, G. Jonsson, A. S. Meyer. Predicting optimal back-shock
1005 times in ultrafiltration hollow fiber modules through path-lines. Journal of Membrane Science,
1006 470 (2014) 275-293.
1007 [117] E. Akhondi, F. Zamani, A. W. K. Law, W. B. Krantz, A. G. Fane, J. W. Chew. Influence of
1008 backwashing on the pore size of hollow fiber ultrafiltration membranes. Journal of Membrane
1009 Science, 521 (2017) 33-42.
1010 [118] I. Bouhid de Aguiar, M. Meireles, A. Bouchoux, K. Schroen. Microfluidic model systems
1011 used to emulate processes occurring during soft particle filtration. Scientific Reports, 9 (2019)
1012 3063.
1013 [119] M. Loginov, F. Samper, G. Gesan-Guiziou, T. Sobisch, D. Lerche, E. Vorobiev.
1014 Characterization of membrane fouling via single centrifugal ultrafiltration. Journal of the Taiwan
1015 Institute of Chemical Engineers, 94 (2019) 18-23.

[120] M. Zhou, H. Sandstrom, M.-P. Belioka, T. Pettersson, T. Mattsson. Investigation of the cohesive strength of membrane fouling layers formed during cross-flow microfiltration: The effects of pH adjustment on the properties and fouling characteristics of microcrystalline cellulose. Chemical Engineering Research and Design, 149 (2019) 52-64.

[121] A. Bouchoux, P. Qu, P. Bacchin, G. Gesan-Guiziou. A general approach for predicting the filtration of soft and permeable colloids: The milk example. Langmuir, 30 (2014) 22-34.

[122] C. Broyard, F. Gaucheron. Modifications of structures and functions of caseins: a scientific and technological challenge. Dairy Science and Technology, 95 (2015) 831-862.

[123] C. G. K. De Kruif, T. Huppertz. Casein Micelles: Size distribution in milks from individual cows. Journal of Agricultural and Food Chemistry, 60 (2012) 4649-4655.

[124] G. A. Morris, T. J. Foster, S. E. Harding. Further observations on the size, shape, and hydration of casein micelles from novel analytical ultracentrifuge and capillary viscometry approaches. Biomacromolecules, 1 (2000) 764-767.

[125] A. Bouchoux, P.-E. Cayemitte, J. Jardin, G. Gesan-Guiziou, B. Cabane. Casein micelle dispersions under osmotic stress. Biophysical Journal, 96 (2009) 693-706.

[126] A. Bouchoux, B. Debbou, G. Gesan-Guiziou, M.-H. Famelart, J.-L. Doublier, B. Cabane. Rheology and phase behavior of dense casein micelle dispersions. Journal of Chemical Physics, 131 (2009) 165106.

Figure captions

Fig. 1. Liquid p_l and solid p_s pressures (dashed and solid curves, respectively) in a system of a particulate filter cake on a membrane surface at the moments (a) before and (b) after the release of filtration pressure ΔP; arrows show the liquid flow direction. The initial solid pressure in the cake psi varies from the membrane-cake ($\omega = 0$) to the cake-suspension interface ($\omega = \omega_0$), where is ω the material coordinate. For colloidal objects, distribution of the local osmotic pressure π in cake and suspension is equivalent to distribution of p_s in particulate filter cake, while the liquid pressure p_l is not determined.

Fig. 2. Solid pressure distribution during the swelling of a thick filter cake ($\omega_0 = 100$ μm) formed at the membrane surface with $r_m = 10^{13}$ m^{-1}: (a) without filtrate inflow across the membrane ($r_{in} = \infty$); (b) with filtrate inflow across the membrane with $r_{in} = 10^{13}$ m^{-1}. The time after the pressure release (in seconds) is shown near the curves.

Fig. 3. Solid volume fraction distribution during the filter cake swelling: (a) thick filter cake without filtrate inflow across the membrane ($r_{in} = \infty$); (b) thick filter cake with filtrate inflow across the membrane with $r_{in} = 10^{13}$ m^{-1}; (c) thin filter cake with filtrate inflow across the membrane with $r_{in} = 10^{13}$ m^{-1}. The time after the pressure release (in seconds) is shown near the curves; in each case $r_m = 10^{13}$ m^{-1}.

Fig. 4. Solid volume fraction at the cake-membrane interface versus the swelling duration for the thick filter cake (example for $\omega_0 = 100$ μm) for different values of outside-in membrane resistance r_{in} (shown near the curves). The inside-out membrane resistance is $r_m = r_{in}$ (except of $r_m = 10^{13}$ m^{-1} for $r_{in} = \infty$). Dashed horizontal corresponds to the concentration of sol-gel transition φ_{sg} for the studied system.

Fig. 5. Time required for filter cake swelling θ at different conditions: (a) θ versus the membrane hydraulic resistance r_m for thin ($\omega_0 = 10$ μm, dashed curves) and thick ($\omega_0 = 100$ μm, solid curves) filter cakes for the cases with ($r_{in} = r_m$, curves) and without ($r_{in} = \infty$, horizontals) filtrate inflow across the membrane; (b) θ versus the filter cake thickness ω_0 and initial filter cake resistance r_{ci} for the cases with (example for $r_{in} = 10^{13}$ m^{-1}) and without ($r_{in} = \infty$) filtrate inflow across the membrane with $r_m = 10^{13}$ m^{-1}.

Fig. 6. To the experiment on membrane rinsing after the cake swelling: filter cakes with different particle concentration distribution (cake 1 with $\varphi_m > \varphi_{sg}$ and cake 2 with $\varphi_m < \varphi_{sg}$);

dashed horizontal corresponds to the concentration of sol-gel transition, φ_{sg}, shaded parts can be removed from the surface (at left) by small tangential force, because $\varphi \le \varphi_{sg}$ at their left borders.

Fig. 7. Relative residual cake resistance r_r/r_{ci} when the sweeping force is applied after the swelling duration t in the absence (solid curves $r_{in} = \infty$) and presence (dashed curves, $r_{in} = r_m$) of filtrate inflow across the membrane: (a) thin filter cakes, $\omega_0 = 10$ μm; (b) thick filter cakes, $\omega_0 = 100$ μm. The values of r_m are shown near the curves.

Fig. 8. Solid concentration distribution $\varphi(x)$ and corresponding yield stress distribution $\tau_0(x)$ in a swelled gel. In the vicinity of membrane the part of the gel with $\tau_0(x) < \tau_{ext}$ can flow under the external shear force, that cause the movement of the denser part of the gel with $\tau_0(x) > \tau_{ext}$.

Fig. 9. Estimated values of the gap thickness h (dashed curves) and the tangential velocity of the gel v (solid curves) versus the swelling duration for (a) thin ($\omega_0 = 10$ μm) and (b) thick ($\omega_0 = 100$ μm) filter cakes under the external tangential shear $\tau_{ext} = 20$ Pa. The values of the membrane resistance to filtrate inflow r_{in} are indicated near the curves. The curves end, when the solid gel disappears because of the swelling: $\varphi_{max} = \varphi(\tau_0 = \tau_{ext})$. Horizontals correspond to the moment of the solid gel disappearance in the absence of filtrate inflow across the membrane: $r_{in} = \infty$, $\varphi_m = \varphi(\tau_0 = \tau_{ext})$.

Fig. C1. Pressure dependency of solids volume fraction and specific filtration resistance for aqueous dispersions of casein micelles (calculated from the data reposted by Bouchoux et al. [121]). Dotted vertical corresponds to the solid pressure in the point of sol-gel transition; dashed vertical corresponds to the solid pressure required for “irreversible” gel formation.

Fig. C2. Values of parameters of Herschel-Bulkley model for casein micelles dispersions at different solid concentrations: symbols – data obtained by least-square fitting of experimental dependencies $\tau(\dot{\gamma}, \varphi)$ (presented by Jin at al. [83]) with the help of Eq. (C3), curves – result of best curve fitting for these data. Dotted vertical corresponds to the concentration of sol-gel transition.